Studies on Optoelectronic Properties of Structurally Confined Conjugated Molecules and Molecular Aggregates

Yusuke Hattori

Preface

The present thesis is the summary of the author's studies from 2016 to 2022 at the Department of Molecular Engineering, Graduate School of Engineering, Kyoto University under the University under the supervision of Professor Shu Seki.

The purpose in this thesis is to clarify the correlation between the configuration/conformation and the optoelectronic properties of conjugate polymer and oligomer.

Yusuke Hattori

Kyoto, July 2022

Contents

General Introduction

1.1 Conjugated polymer

The polymer, also called a macromolecule, is molecular consisting a series of repeating units connected by covalent bonds. While the entropy for small molecule can be defined only in systems of multiple molecules, the entropy for a single polymer chain can be defined because single chain can take on various configuration. When considering the aggregation structures and optoelectrical properties of polymer materials in the condense phase, it is important to primarily gain a deep understanding of the characteristics of single chains.

For example, a flexural polymer such as polyethylene, the configuration of the polymer chain changes with the rotation on the bond angle of the carbon-carbon single bond. Therefore, an analysis of the rotation potential is essential for understanding the configuration of polymer. Polyethylene have three stable states due to steric hindrance caused by carbon and hydrogen atoms, in the case of a polymer chain with a degree of polymerization of N, there are 3^N configuration. The persistence length q is parameter of molecular chain stiffness. Most of the widely used amorphous polymers have a random-coil with an average of q less than 1 nm.[1] On the other hand, conjugated polymers have rigid backbone derived from π-conjugated structure. Conjugated polymer is energetically most stable when the monomer units are aligned in the same plane due to delocalization of π-electrons through polymer chain. Therefore, conjugated polymer chains have fewer rotational isomers and longer the persistence length than flexural polymers. Longer

persistence length means a larger radius of gyration relative to the molecular weight, which results in a larger absorption cross section of the segment. The absorption cross section is an extremely important factor in discussing the light absorption and emission process of a material. Long persistence length are the basis of the unique optoelectronic properties of conjugated polymer materials.

Conjugated polymers have attracted much attention due to their charge transport and luminescence properties. The charge transport properties of organic semiconductors were first reported for charge-transfer complexes of perylene by Akamatsu et al.[2] Polyacetylene (PA) as well as perylene is substructure of graphite. It was thought that electrons could easily move along the main chain consisting of conjugated double bonds. However, a Peierls transition: a metal-insulator phase transition occurs in one-dimensional π-conjugated electron systems when electron-lattice interactions are strong.[3] Various π-electron conjugated polymers were synthesized and their conductivities were measured until the late 1970's, unfortunately, charge carrier conductivities were only about 10^{-6} Scm^{-1} at most. PA showed drastically increase of charge carrier conductivity by iodine doping, and research in this field was greatly stimulated.[4.5] The energetic status of such charged species were also well considered with very sophisticated theoretical approaches started from well–known Su–Schrieffer–Heeger Hamiltonian.[6.7]

PA becomes an insoluble solid with elongation chain length, and the polymer chains could not be completely aligned. Incorporation of side chains to the conjugated polymers has been indispensable to afford solubility of the polymers in organic solvents, however the entropic gain by the side chains is in a trade-off for the stabilization of conjugated polymer backbones.[8] It is still unclear to obtain methodologies to access target aggregation structures.

1.2 The coil-to-rod-like transition

Because polymer chains arrangement on solid state is complex and heterogeneous, the disorder of electronic states are problems when conjugate polymers are applied to electronic devices as optoelectronic materials.[9-12] The configuration of polymers in solution has significant impact on the aggregation structure, which is often reflected by that the structure in solid films prepared by solution processes. [13-14] Therefore, it is essential to understand the aggregation of polymer chains in the liquid phase for deep insights on the aggregation morphology of polymer films. The polymer chain in solution realizes an enormous number of possible configurations and their distribution follows the Boltzmann statistics. In many cases, polymers take a coiled form and are called random coils. There are two forces acting between monomers in solution, the remote interactions and the excluded volume effect. Below the theta temperature where the two forces are balanced, or in poor solvents than theta solvents, the phase transition from a random coil state to a globule-like state occurs. This is so called coil-globule transition. However, in the case of conjugated polymers with small flexibility of polymer chains backbones, the transition is different from the coil-to-globular transition. In the case of rigid polymers, the number of monomer units consisting one segment increases when the transition occurs at low temperatures.[8] Unlike the globular state, the conjugate polymer chains form highly ordered rod-like aggregates, which is called the coil-to-rod-like transition.

1.3 Correlation between configuration/conformation and optoelectronic properties

Optoelectronic properties of organic semiconductor can be tuned by changing chemical structure of π-conjugate core. Even if conjugate polymer have the same monomer structure, their electronic states differ greatly depending on the bonding mode. Variation in bonding mode causes

stereological disorder in the polymer chain. For example, polythiophene(PT) have long been studied among conjugated polymers and have been demonstrated that their optoelectronic properties are strongly affected by the regioregularity of the thiophene units,[15] and head-to-tail (HT) polymers are superior to head-to-head (HH) and regiorandom isomers.[16] Regioregular polythiophene (RR-PT) form lamellar structures in thin films due to strong intermolecular interactions, and high FET hole mobility (~10^{-1} $cm^2V^{-1}s^{-1}$) has been reported.[17] In PT, efficient intermolecular charge transport induced by stereo-regular side chains and intramolecular charge transport on rigidly elongated main chains is important.[18]

The photoelectronic properties of conjugated polymers are strongly influenced by not only chemical structure but also configuration. The monomer units of conjugated polymers are energetically stabilized by the delocalization of π-electrons, however conjugated polymers in solvent or in a molten state have segment length distribution due to the effects of thermal fluctuation and steric hindrance. When the number of units with delocalized π-electrons changes, the electronic states change accordingly. The redshift in the maximum absorption wavelength and an increase of absorption coefficient in the electronic absorption spectra was confirmed in poly(p-phenylene vinylene (PPV) oligomers experiment.[19] The conversion in electronic states due to an increase in the planarity between monomer units is well known in the α-β phase transition of poly (9,9-dioctylfluorene)(PFO).[20-21] PFO monomer units cannot be arranged in the same plane due to a steric effect of the hydrogen atom of the benzene ring. PFO have α-phase with a dihedral angle of 135 degrees and more planar β-phase with a dihedral angle of 165 degrees.[22] In β-phase, a new peak is observed on the longer wavelength side at absorption spectra by temperature modulation and mixing solvents. Thus, the planarization: the configuration change are closely related with photoelectronic properties. Intramolecular and intermolecular interactions play important role

during planarization process of polymer chains, intramolecular and intermolecular interactions on electronic states an important insight for the fabrication of more ordered polymer aggregates.

1.4 Electronic coupling between monomers

The vibrational structure of the absorption and fluorescence spectra can provide insight into the electronic couplings of neighboring molecules. The Franck-Condon (FC) transition of the absorption spectrum $\bar{A}(\hbar\omega)$ and fluorescence spectrum $\bar{S}(\hbar\omega)$, including the intramolecular vibration mode i, can be modeled by Equations 1 and 2.[23]

$$\bar{A}(\hbar\omega) = n(\hbar\omega)\sum_{\{m_i\}}\prod_i I_{0\to m_i} \times \Gamma\left[\hbar\omega - \left(\hbar\omega_{0\to 0} + \sum_i m_i\hbar\omega_i\right)\right], \qquad (1)$$

$$\bar{S}(\hbar\omega) = n^3(\hbar\omega)^3\sum_{\{m_i\}}\prod_i I_{0\to m_i} \times \Gamma\left[\hbar\omega - \left(\hbar\omega_{0\to 0} + \sum_i m_i\hbar\omega_i\right)\right], \qquad (2)$$

where ω_i is the frequency of the i-th mode, m_i=0,1,2,... is the vibration quantum number in the i-th mode, and Γ is a Gaussian function.

The intensity of the 0⟶m_i vibration transition $I_{(0\to mi)}$ is related to the Huang-Rhys parameter S_i[24] in Equation 3.

$$I_{0\to m_i} = e^{-S_i}\, {S_i}^{m_i}/m_i!, \qquad (3)$$

The Huang-Rhys parameter *S* is the average number of phonons emitted when the exciton relaxes to the lowest excited level, indicating the magnitude of the electron-orbit interaction.[25]

$$S = \frac{M\omega}{2\hbar}(\Delta Q)^2, \qquad (4)$$

where m^* and $\hbar$ are the effective mass of an electron and Dirac's constant, respectively.[24,26–31] The Huang-Rhys parameter *S* can be derived easily and experimentally by (Equation 5),

$$S = I_{0-1}/I_{0-0}, \qquad (5)$$

where $I_{0\text{-}0}$ and $I_{0\text{-}1}$ are the intensities of the 0-0 and 0-1 transitions.

The theoretical background of the correlation between aggregation morphology and optical properties in conjugated polymers was developed by Spano et al.[32-34] based on the exciton model of small molecules proposed by Kasha.[35.36]In the case of two different dye molecules form a dimer, their optical properties significantly depend on intermolecular interactions. In the dimer, the electron distribution of one molecule is affected by the electron distribution of the other. Since the two dye molecules are stabilized by the van der Waals interaction, the electronic levels shift by ΔD = D - D′, also called "gas-to-crystal shift," and further split by a resonance energy β, which is also called "gas-to-crystal shift".(Figure 1)

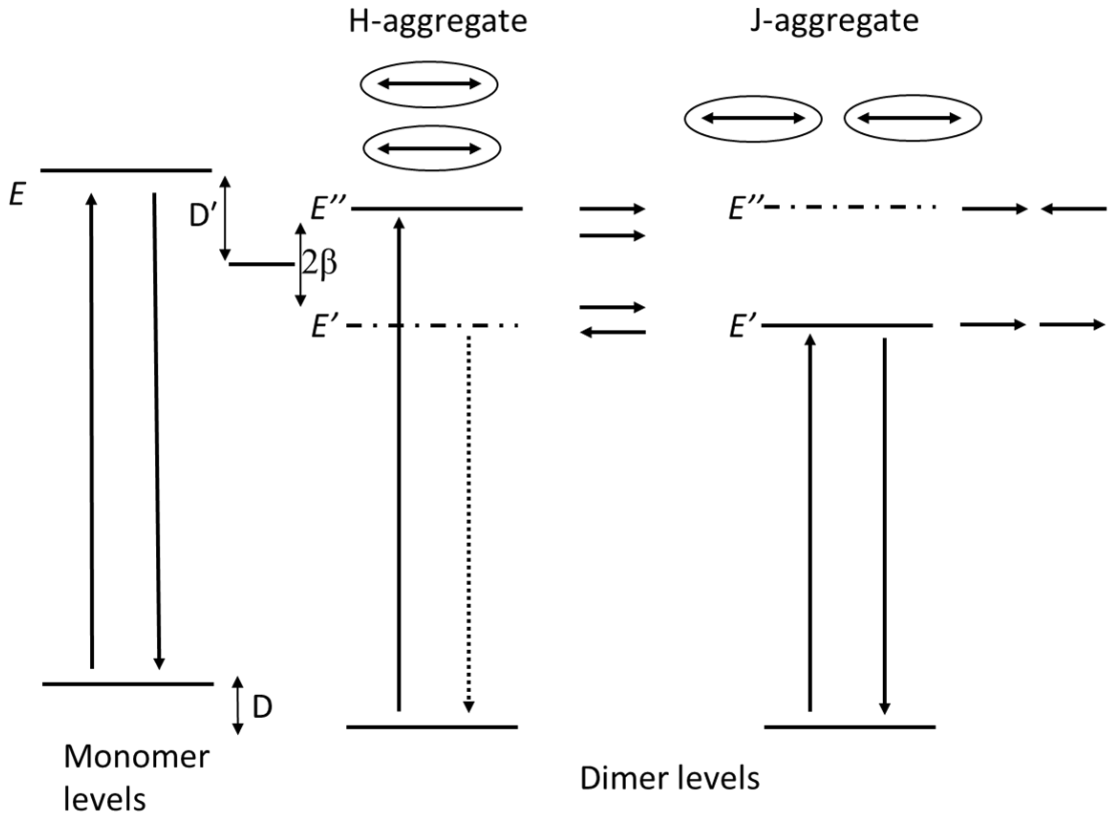

Figure 1. Illustration of the different energetic shifts and splitting of the energy levels occurring for the formation of an ideal dimer. The corresponding relative orientations of the transition dipoles for two limiting cases are indicated as arrows.

Depending on the orientation of the two molecules, the two molecules are roughly classified into two types according to their orientation: H-type (Hypsochromically shifted) and J-type (J for Jelly, one of the first workers who investigated these shifts) [37]. Since the transition dipole moment is given by the vector sum of the individual dipole moments, in the H-type case, the transition dipole moments cancel each other at the low energy side and the transition is forbidden, but only the high energy side is an allowed transition. On the other hand, in the case of J-type, only the low energy side becomes an allowed transition, and the high energy side becomes a forbidden transition. J-type aggregate lead to spectral red-shift, and narrowing of the 0-0 vibronic transition, and increased 0-0 to 0-1 vibronic peak ratio (Huang-Rhys parameter *S*). In conjugate polymers, J-type coupling occurs predominantly along the same polymer chain backbone, because of the covalent interactions between the head-to-tail arranged transition dipole moments of the monomer units. As the planarity of the chain improves, J-type coupling becomes stronger and experimentally Huang-Rhys parameter *S* decrease.

The exciton interactions of conjugated polymers in aggregate state are different from those of small molecules.[38-40] Because neighboring dye molecules are covalently linked, it is difficult to unambiguously distinguish between J-type and H-type aggregates. Intramolecular defects such as kinks and twists are always present in conjugated polymers, which disrupt the π-conjugation of the main chain backbone. When the transition dipole moments are aligned along the same line due to intramolecular configurations, the characteristics of J-type coupling are more strongly reflected. In contrast, the H-type coupling is basically caused by intermolecular interaction (the alignment of π-planes between different molecular chains). Assuming a one-dimensional conjugated polymer, the molecular chains aligned in parallel induce not only H-type coupling but also J-type coupling. In fact, in the crystal domains of RR-P3HT[41], the polymer backbone is stacked and π-stacked due

to π-π interactions, and the monomers form a J-type arrangement by planarization within the molecular chain. At the same time, the polymer chains also have H-type conformation, so the electronic levels are strongly influenced by both J-type and H-type. It is impossible to separate H-type and J-type coupling in conjugate polymer aggregation. Experiment of conjugate polymer dispersed in polypropylene could avoid H-type coupling, but no planarization occurred. In addition, due to rigidity of conjugated polymer backbones, degrees of freedom on segment is low and it is difficult to rearrange when incorporated into crystals. The disordered aggregate structure induces confusion in the electronic coupling.

Insulated Molecular Wires (IMWs) is a type of conjugate polymer, whose π-conjugate backbones be molecularly "insulated" by molecular design.[42] Sophisticated molecular design have not only insulated molecular chains by steric hindrance, but also inhibited monomer twisting by controlling configuration.[43,44] IMWs applied a ring structure achieved the long effective conjugation length and showed J-type characteristics specifically. Because IMWs is insulator on a macroscopic level, single polymer chain charge transport properties cannot be evaluated by direct-current (DC) method. The flash photolysis-time-resolved microwave conductivity (FP-TRMC) measurement technique is a contactless evaluation method.[45,46] In FP-TRMC, transient charge carrier injected into the domains via photoionization, and carrier mobility precisely measured as the microwave dielectric loss in this material. FP-TRMC method prove the charge carrier mobility along a single planar backbones of IMWs. IMWs based on polythiophene backbone showed in an excellent intrawire hole mobility of 0.9 $cm^2\ V^{-1}\ s^{-1}$.[43] The high hole mobility was achieved by order electron state, insulate structure induced planarization of conjugate backbones and prevented order electronic states from intermolecular electron coupling.

2.1 Poly-(p-phenyleneethynylene)

Poly-(*p*-phenyleneethynylene) (PPE) is one of simplest conjugate polymer, phenylene rings are separated by alkyne linker. PPE have planer main chain backbone than polyphenylene (PP), because alkyne linker prevents steric effect between hydrogen atoms on phenyl rings. PPE is generally synthesized by Sonogashira-Hagiwara coupling to react an aromatic diyne with aromatic dihakide in an amine solvent. High molecular weight PPE obtained when diiodearenes are utilized in mixture of triethlyamine and THF as solvent and $Pd(PPh_3)_4$ as catalyst in combination with CuI.[47]

PPE has attracted much attentions due to its feasibility in organic electronic devices. The conjugation length is strongly affected by the configuration/rotation of the respective phenyl rings in a PPE main chain. One of the most appealing attributes of PPE comes from the efficient electronic communication that occurs along their linearly conjugated structures. This effect can be attributed to the cylindrical symmetry of alkyne linker, which is able to maintain conjugation between adjacent phenyl groups regardless of the relative orientations of their aromatic planes. [48-50] Consider tolane as an example, the rotation potential for isolate molecule depends on conjugation between phenyl rings.[51] Acetylene has two p orbitals perpendicular to the molecular axis that share an electron with each other. A planer equilibrium geometry may result from overlapping pπ–orbitals of phenyl rings with same pπ–orbitals of alkyne linker. Interaction of another pπ–orbitals of alkyne linker would stabilize the perpendicular molecular form. From calculation of the total electron energies for two conformation of tolane, the planar structure is more stable than the perpendicular one (ΔE=0.03β=-0.6 kcal mol^{-1}). The small difference in energy indicates unhindered rotation. The relatively free rotation on alkyne-aryl single bonds leads to the coexistence and rapid equilibration of coplanar and twisted structures.

Several PPE derivative with different side chains were synthesized to control π-conjugate backbone configuration, and measured their conductivity. Undoped 2,5-dialkyloxy-PPEs exhibited electrical conductivity of the order of ~10^{-9} S cm^{-1}.[52.] This result is not higher compared to other conjugate polymer, rotation on alkyne-aryl single bonds would disturb aggregation and electron state. If rotation of backbone could be suppressed through aggregation process, PPE would have coherent electron states on the order π-conjugate backbones.

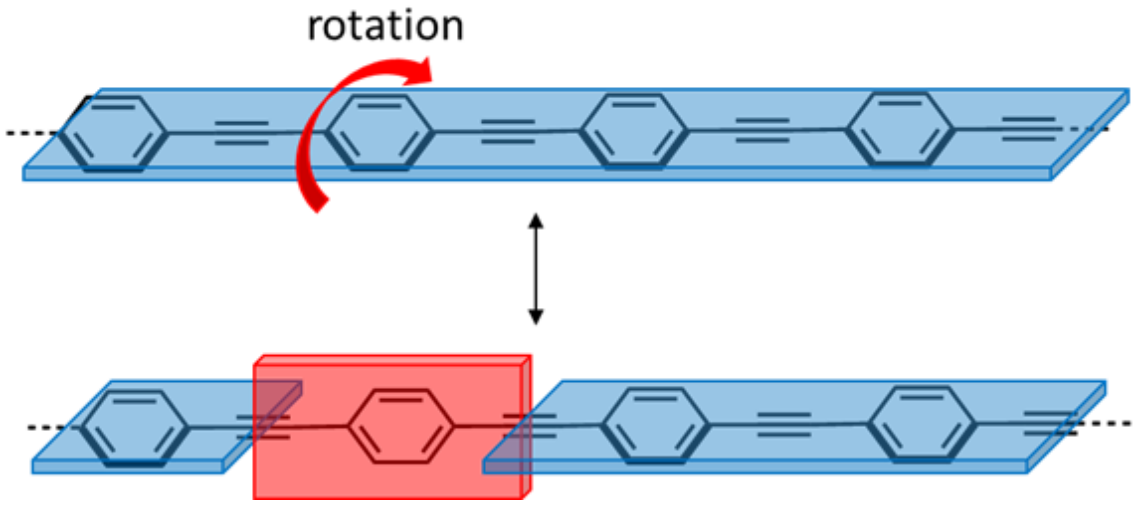

Figure 2. The Structure of PPE and rotation dynamics on alkyne-aryl single bonds.

2.2 Poly(cyclopentenylene-vinylene)（PCPV）

PAs, the oldest and simplest conjugated backbones were synthesized in 1971 by Shirakawa and co-workers.[4,5]As seen in the giant leap in electronic conductivity upon chemical doping into polyacetylene, the conjugated backbones have been recognized as an efficient platform for the charge carrier transport, pioneering to the first flexible electronic materials based on macromolecular systems. However, the precise control of backbone configuration had not been addressed because of their extremely low solubility against any solvents. Olefin metathesis catalysts are particularly effective for producing conjugated polyenes with excellent control over molecular weight and narrow dispersity.[53-56] However cyclopolymerization of 1,6-heptadiyne derivatives via the olefin metathesis reaction provide regiochemical outcome, cyclopentenylene-vinylene alternating repeat units, methylidene-cyclohexene repeat units, or a random mixture of the two units. Many efforts have been made to synthesize with regioselectivy polymerization to

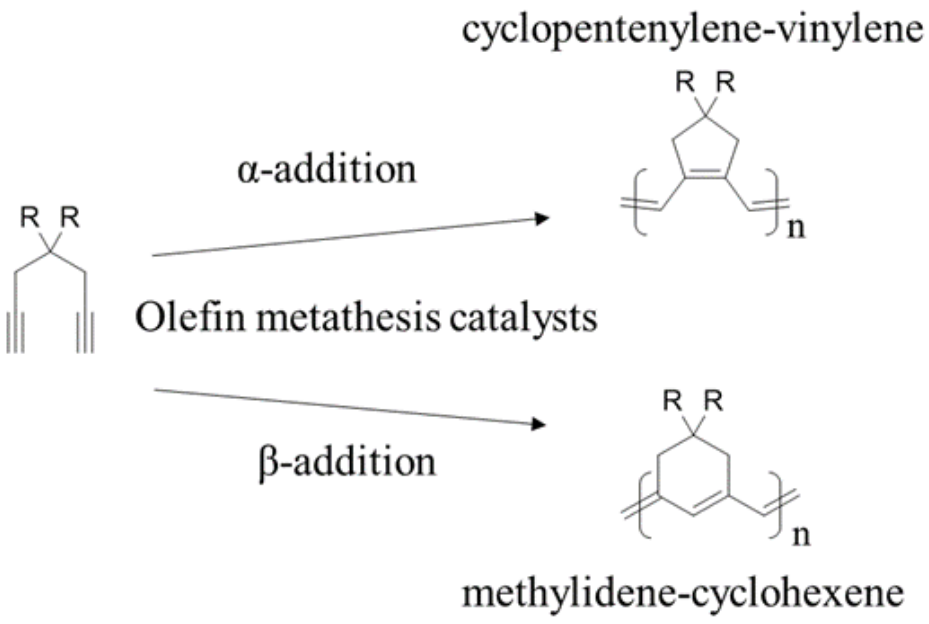

Figure 3. Two Possible Pathways for the Cyclopolymerization of 1,6-Heptadiynes

expand the scope of this polymerization. Choi et al. succeeded in synthesizing soluble substituted PCPV by living cyclopolymerization of 1,6-heptadiyne derivatives via the olefin metathesis reaction promoted by the third-generation Grubbs catalyst.[57–63] This sophisticated living cyclopolymerization produce selectively conjugated polymers composed of 5-membered-ring structures with excellent control over molecular weight and polydispersity index. Because side chains attached to the spiro carbon in a five-membered ring prevent π-conjugate backbones from oxidation in the atmosphere, PCPV is more stable than other PAs derivertive. Perpendicular side chain to backbone and five-membered ring eliminate π-staking on aggregate state, thus PCPV is can be regarded as a kind of IMWs. The author assume that PCPVs is good platform for exploration on one dimensional π-conjugate backbone and their configuration can be tuned by side chain design.

Reference

(1) P.J. Flory, "*Statistical Mechanics of Chain Molecules*", Wiley Interscience, NewYork, (1969)

(2) H. Akamatsu, H. Inokuchi, Y. Matsunaga, *Nature*, (1954) **173**, 168.

(3) E. Peierls: *Quantum Theory of Solids*, Cleredon Press, Oxford (1955)

(4) H.Shirakawa, S.Ikeda, *Polym. J.* (1971), **2**, 231−244.

(5) H.Shirakawa, E. J.Louis, A. G.MacDiarmid, C. K. Chiang, A. J. Heeger, *J. Chem. Soc., Chem. Commun*. (1977), 578−580.

(6) P. Su. W, J. R. Schrieffer, A. J. Heeger, *Phys. Rev. Lett.* (1979), **42**, 1698−1701.

(7) P. Su. W, J. R. Schrieffer, A. J. Heeger, *Phys. Rev. B* (1980), **22**, 2099−2111.

(8) A. Kolinski, J. Skolnick, R. Yaris, J. Chem. Phys., (1986), **85**, 3585-3597.

(9) Y. Liu, J. Zhao, Z. Li, C. Mu, W. Ma, H. Hu, K. Jiang, H. Lin, H. Ade and H. Yan, Nat. Commun. (2014), **5**, 5293.

(10) J. F. Chang, B. Sun, D. W. Breiby, M. M. Nielsen, T. I. Sölling, M. Giles, I. McCulloch and H. Sirringhaus, *Chem. Mater.* (2004), **16**, 4772−4776.

(11). H. Sirringhaus, P. J. Brown, R. H. Friend, M. M. Nielsen, K. Bechgaard, B. M. W. Langeveld-Voss, A. J. H. Spiering, R.A. J. Janssen, E. W. Meijer, P. Herwig and D. M. de Leeuw, *Nature*, (1999), **401**, 685−688.

(12) R. J. Kline, M. D. McGehee, E. N. Kadnikova, J. Liu and J.M. J. Fréchet, *Adv. Mater.* (2003), **15**, 1519−1522.

(13) S. Seki, S. Tsukuda, K. Maeda, S. Tagawa, H. Shibata, M. Sugimoto, K. Jimbo, I. Hashitomi, and A. Kohyama *Macromolecules*, (2005), **38**, 10164-1017010.

(14) S.Seki, S.Tsukuda, S.Tagawa, M.Sugimoto, *Macromolecules*, (2006), **39**, 7446.

(17) H. Sirringhaus, N. Tessler, R. H. Friend, *Science*, (1998), **280**, 1741.

(18) A. Saeki, S. Ohsaki, S. Seki, S. Tagawa, *J. Phys. Chem. C*, (2008), **112**, 16643.

(19) H. Meier. Diplomarbeit, I*nstitut fur Physikalische Chemie, Universitat Mainz*, (1981)

(20) T. Li Long Huang, Zeming Bai, Xiaona Li, Bo Liu, Dan Lu, *Polymer*, (2016), **88**, 71-78

(21) L Huang, X. Huang, G. Sun, C. Gu, D. Lu, and Y. Ma, *J. Phys. Chem. C*, (2012), **116**, 7993−7999.

(22) L. Huang, L.L. Zhang, X.N. Huang, T. Li, B. Liu, D. Lu, *J.Phys. Chem. B*, (2014), **118**, 791.

(23) P. K. H. Ho, J.-S. Kim, N. Tessler, and R. H. Friend, *J. Chem. Phys.* (2001), **115**, 2709–2720

(24) K. Huang and A. Rhys, *Proc. R. Soc. London, Ser. A* (1950), **204**, 406– 423.

(25) Heinz. Bässler and Bernd. Schweitzer, *Acc. Chem. Res.*, (1999), **32**, 173-182.

(26) K. Pichler, D. A. Halliday, D. D. C. Bradley, P. L. Burn, R. H. Friend, A. B. Holmes, *J. Phys.: Condens. Matter*, (1993), **5**, 7155− 7072.

(27) Z. Shuai, J. L. Bredas, W. P. Su, *J. Chem. Phys. Lett.* (1994), **228**, 301−306.

(28) J. Cornil, D. Beljonne, Z. Shuai, T. W. Hagler, I. Campbell, D. D. C. Bradley, J. L. Bredas, C. W. Spangler, K. Müllen, *Chem. Phys. Lett.*, (1995), **247**, 425−432.

(29) J. W. Blatchford, S. W. Jessen, L. B. Lin, T. L. Gustafson, D. K. Fu, H. L. Wang, T. M. Swager, A. G. MacDiarmid, A. Epstein, *J. Phys. Rev. B*, (1996), **54**, 9180−9189.

(30) J. Yu, M. Hayashi, S. H. Lin, K K. Liang, J. H. Hsu, W. S. Fann, C. I. Chao, K. R. Chuang, S. A. Chen, *Synth. Met.*, (1996), **82**, 159−166.

(31) S. Quan, F. Teng, Z. Xu, L. Qian, T. Zhang, D. Liu, Y. Hou, Y. Wang, X. Xu, *J. Lumin.*, (2007), **124**, 81−84.

(32) H. Yamagata and F. C. Spano, *J. Chem. Phys.*, (2011), **135**, 054906.

(33) H. Yamagata and F. C. Spano, *J. Chem. Phys.*, (2012), **136**, 184901.

(34) H. Yamagata and F. C. Spano, *J. Phys. Chem. Lett.*, (2014), **5**, 622−632.

(35) M. Kasha, *Radiat. Res.*, (1963), **20**, 55−70.

(36) M. Kasha, H. Rawls and M. Ashraf El-Bayoumi, *Pure Appl. Chem.*, (1965), **11**, 371−392.

(37) E. E. Jelley, *Nature*, (1936), **138**, 1009−1010.

(38) F. Panzer, H. Bässler, and A. KöhlerD. *J. Phys. Chem. Lett.*, (2017), **8**, 114−125

(39) M. Baghgar, J. A. Labastide, F. Bokel, R. C. Hayward, and M. D. Barnes, *J. Phys. Chem. C*, (2014), **118**, 2229−2235.

(40) T. Eder, T. Stangl, M. Gmelch, K. Remmerssen, D. Laux, S. Höger, J. M. Lupton and J. Vogelsang, *Nature Communications*, (2017), **8**, 1641.

(41) F. Panzer, H. Bässler, R. Lohwasser, M. Thelakkat, and A. Köhler, *J. Phys. Chem. Lett.*, (2014), **5**, 2742−2747.

(42) C. Pan, C. Zhao, M. Takeuchi, and K. Sugiyasu, Chem. Asian J., (2015), **10**, 1820 – 1835

(43) K. Sugiyasu, Y. Honsho, R. M. Harrison, A. Sato, T. Yasuda, S. Seki, and M. Takeuchi, *J. Am. Chem. Soc.*, (2010), **132**, 14754–14756.

(44) J. Terao, A. Wadahama, A. Matono, T. Tada, S. Watanabe, S. Seki, T. Fujihara, and Y. Tsuji, *Nature Commun.*, (2013), **4**, 1691.

(45) A. Saeki, S. Seki, T. Sunagawa, K. Ushida, S. Tagawa, *Philos. Mag.*, **86**, (2006), 1261.

(46) A. Saeki, S. Seki, Y. Koizumi, and S. Tagawa, *J. Photochem. Photobiol., A* **186**

(47) Q. Zhoz, T.M.Swager, *J. Am. Chem. Soc.*, (1995), **117**, 12593–12602.

(48) M. Levitus, K. Schmieder, H. Ricks, K. D. Shimizu, U. H. F. Bunz,and M. A. Garcia-Garibay, *J. Am. Chem. Soc.*, (2001), **123**, 4259-4265

(49) Carrie E. Halkyard, Mary E. Rampey, Lioba Kloppenburg, Shannon L. Studer-Martinez, and Uwe H. F. Bunz, *Macromolecules*, (1998), **31**, 8655–8659

(50) Tzenka Miteva, Liam Palmer, Lioba Kloppenburg, Dieter Neher, and Uwe H. F. Bunz, *Macromolecules*, (2000), **33**, 652–654

(51) A. V.Abramenkov, A. Almenningen, B. N. Cyvin, S. J. Cyvin, T. Jonvik, L. S. Khaikin, C. Rommingin, L. V. Vilkov, *Acta Chem. Scand.I,* (1988), **A42**, 674−678.

(52) R. Pizzoferrato, M. Berliocchi, A. Di Carlo, P. Lugli, M. Venanzi, A. Micozzi, A. Ricci, and C. Lo Sterzo, *Macromolecules*, (2003), **36**, 2215–2223

(53) S.-K. Choi, Y.-S. Gal, S.-H. Jin, H. K. Kim, *Chem. Rev.*, (2000), **100**, 1645−1682.

(54) R. H. Grubbs, *Angew. Chem., Int. Ed.*, (2006), **45**, 3760−3765.

(55) A. H. Hoveyda, A. R. Zhugralin, *Nature*, (2007), **450**, 243−251.

(56) C. W. Bielawski, R. H. Grubbs, *Prog. Polym. Sci.*, (2007), **32**, 1−29.

(57) E. H. Kang, I. S. Lee, T. L. Choi, *J. Am. Chem. Soc.*, (2011), **133**, 11904−11907.

(58) E.-H. Kang, I.-H. Lee, T.-L. Choi, *ACS Macro Lett.*, (2012), **1**, 1098−1102.

(59) E. H.Kang, T. L. Choi, *ACS Macro Lett.*, (2013), **2**, 780−784.

(60) E. H. Kang, S. Y. Yu, I. S. Lee, S. E. Park, T. L. Choi, *J. Am. Chem. Soc.*, (2014), **136**, 10508−10514.

(61) H. Jung, K. Jung, M. Hong, S. Kwon, K. Kim, S. H. Hong, T. L. Choi, M. H. Baik, *J. Am. Chem. Soc.*, (2018), **140**, 834−841.

(62) I. Choi, S. Yang, T. L. Choi, *J. Am. Chem. Soc.*, (2018), **140**, 17218−17225.

(63) G. I. Peterson, S. Yang, T.-L. Choi, *Acc. Chem. Res.*, (2019), **52**, 994−1005.

Chapter 1

Aggregation Dynamics in the Dilute Solution of the Poly(p-phenylene ethynylene) Derivative

1.1 Introduction

The coil-to-rod-like transition of macromolecular chains is one of the most characteristic features of polymeric materials, impacting their major physical properties not only in solutions[1–3] but also in condensed phases.[4,5] Sophisticated methodology has been developed to determine the chain configuration of polymers,[6–8] and it has provided excellent insights into the chain configurations in diluted solutions, polymer melts, and amorphous phases.[9,10] The primary quantitative parameter representing configuration changes of macromolecular chains is the segment persistence length, q. The elongation of q is the prerequisite to suppressing divergence in the configuration and intramolecular entropy in macromolecular systems.[11,12] Rod-like chains with q = 4×10 nm can significantly contribute to the formation of ordered structures of a variety of macromolecular systems and often give high crystallinity in their condensed phases. This is particularly important for the application of macromolecules with electronically-conjugated backbones in organic opto-electronics.[13] Electron stabilization via delocalization over the backbone is advantageous for preserving longer q values in conjugated polymers. However, the stabilization energy is always in

competition with the total free energy of the isolated chains at room temperature.[14] Once the conjugated backbone forms the platform for electronic conducting pathways, excess electrons or holes on the backbone tend to localize on specific sites in the chain with rather higher stabilization energies via vibrational coupling.[15,16] Thus it has been presumed that long q values will be enough to overcome kT, and that they are indispensable for facilitating a highly electronically conductive migrating pathway along the macromolecular chains.

In chapter 1, I have successfully evaluated the dependence of q on T for the simplest linear conjugated backbone: poly-(*p*-phenyleneethynylene) (PPE).[17,18] An abrupt rod-like transition of the PPE backbone was observed as a consequence of the gradual elongation of q upon cooling PPE in solution, resulting in an extremely low energetic disorder in the PPE chains. These results inspired us to propose new protocols to give a highly ordered phase of PPE.

1.2 Experimental Section

Unless otherwise noted, all commercial reagents were purchased from Wako Pure Chemical Industries Ltd., Tokyo Chemical Industry Co. Ltd., or Sigma-Aldrich Co. and used as received. Column chromatography was performed on silica gel 60N (spherical, neutral) from Kanto Chemicals.

The crude polymers were purified by recycling preparative HPLC on a Japan Analytical Industry Co. model LC-9210NEXT equipped with JAIGEL-2.5HH/-3HH columns using CHCl3 as an eluent at a flow rate of 7.5 mL min^{-1}. Molecular weights of polymers were determined by size exclusion chromatography (SEC) in THF calibrated using polystyrene standards. SEC analysis was performed on HITACHI L-2130, L-2455, and L-2530 chromatography instruments with Shodex KF-804L/KF- 805L columns using THF as an eluent at a flow rate of 1 mL min^{-1} at 40°C.

A refractive index detector and multiwavelength photodiode array detector were used for detecting the elution peaks. Electronic absorption spectra were recorded on a JASCO V-570 spectrometer with a Unisoku CoolSpeK UV USP- 203 temperature controller. Photoluminescence spectra were recorded on a HITACHI model F-2700 spectrofluorometer. ^{1}H NMR spectra were recorded by a JEOL model JNM-AL400 spectrometer. Chemical shifts of ^{1}H NMR spectra are determined relative to an internal tetramethylsilane standard (δ) and are given in parts per million (ppm).

Scheme 1. Synthetic Scheme of Poly-*p*-(phenyleneethynylene) (PPE) Derivatives **LPPE**, and **CPPE**

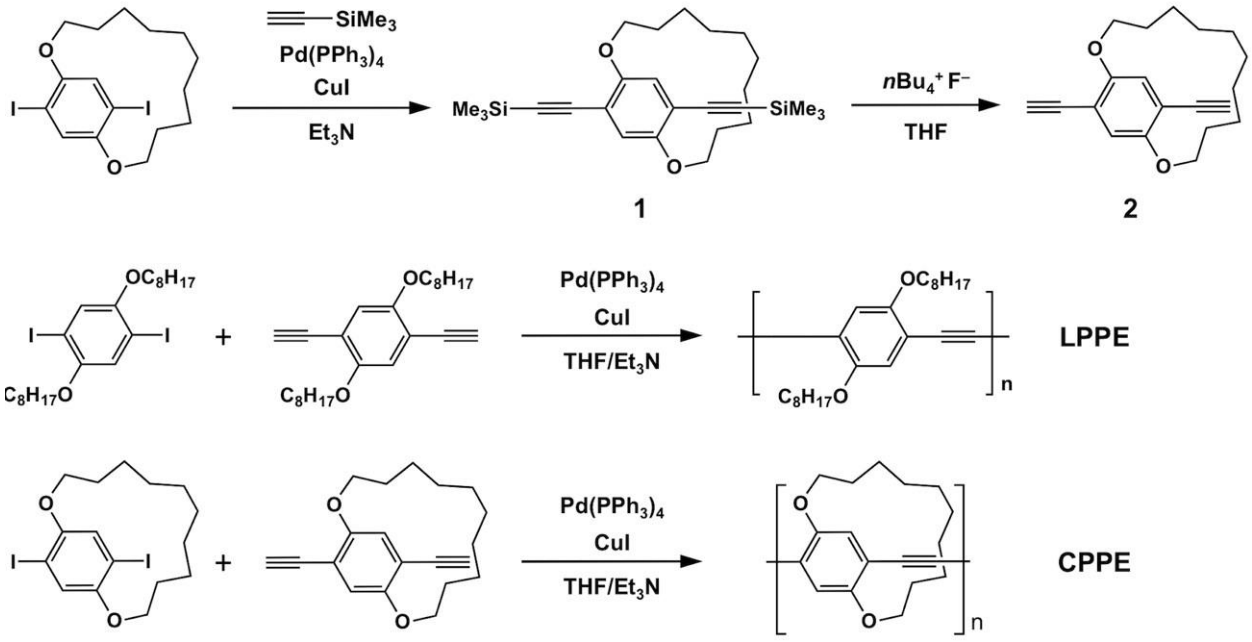

1,4-dioxydecanoxy-2,5-bis(trimethylsilylethynyl)benzene (1)

To a dry Et_3N solution (20 mL) of 1,4-diiode-2,5-oxydecanoxybenzene (500 mg, 1.00 mmol),[S1] $Pd(PPh_3)_4$ (235 mg, 0.20 mmol), and CuI (18 mg, 0.40 mmol) was added trimethylsilylacetylene (547 mg, 3.00 mmol) under N_2, and the mixture was stirred at 60ºC for 12 h. The mixture was

evaporated to dryness under reduced pressure, dissolved in $CHCl_3$, and passed through a plug of SiO_2. The solution was evaporated and purified by chromatography on silica gel eluted with $CHCl_3$/hexane (1/2) to afford 1 as a white solid. Yield: 352 mg (80%). ^{1}H NMR (400 MHz, $CDCl_3$) δ = 7.01 (s, 2H), 4.32 (t, 4H), 1.67 (m, 4H), 1.23 (m, 4H), 0.98 (m, 4H), 0.84 (m, 4H), 0.26 (s, 18H).

1,4-diethynyl-2,5-dioctyloxybenzene (2)

To a dry THF solution (50 mL) of 1 (352 mg, 0.80 mmol) was added a 1 M THF solution of tetrabutylammonium fluoride (2 mL, 2.0 mmol) at 0°C. After stirring for 15 min, the solution was poured into water and extracted with $CHCl_3$. The organic layer was washed with water, dried over $NaSO_4$, filtered, and evaporated to dryness under reduced pressure. The residue was purified by column chromatography on silica gel eluted with $CHCl_3$/hexane (1/2) to afford 2 as a white solid. Yield: 224 mg (95%). ^{1}H NMR (400 MHz, $CDCl_3$) δ = 7.08 (s, 2H), 4.34 (t, 4H), 3.38 (s, 2H), 1.67 (m,4H), 1.23 (m, 4H), 1.01 (m, 4H), 0.79 (m, 4H).

LPPE: Poly(2,5-dioctyloxy-p-phenylene)ethynylene

To a dry Et_3N/THF solution (2.6 mL, 1/1 v/v) of 1,4-diiode-2,5-octyloxybenzene (46 mg, 0.12 mmol) and 1,4-dioctyloxy-2,5-dioctyloxybenzene (71 mg, 0.12 mmol) were added $Pd(PPh_3)_4$ (7.7 mg, 6.0 mmol) and CuI (3.0 mg, 0.010 mmol), and the mixture was degassed by freeze-pump-thaw cycles for 3 times. After stirring at 60°C for 24 h, the mixture was evaporated to dryness under reduced pressure, dissolved in $CHCl_3$, and passed through a plug of SiO_2. Further purification and fractionation were carried out by a recycling preparative SEC using $CHCl_3$ as an eluent. SEC analysis: Mn = 5.2×10^4 g mol^{-1}, Mw = 6.2×10^4 g mol^{-1}, Đ = 1.2.

CPPE: **Poly(2,5-oxydecanoxy-p-phenylene)ethynylene**

To a dry Et_3N/THF solution (7.0 mL, 1/1 v/v) of 1 (87.8 mg, 0.33 mmol) and 2 (96.3 mg, 0.33 mmol) were added $Pd(PPh_3)_4$ (21 mg, 0.017 mmol) and CuI (7.4 mg, 0.034 mmol), and the mixture was degassed by freeze-pump-thaw cycles for 3 times. After stirring at 60 °C for 24 h, the mixture was evaporated to dryness under reduced pressure, dissolved in $CHCl_3$, and passed through a plug of SiO_2. Further purification and fractionation were carried out by a recycling preparative SEC using $CHCl_3$ as an eluent.

SEC analysis: Mn = 1.3×10^4 g mol^{-1}, Mw = 2.3×10^4 g mol^{-1}, Đ = 1.8.

1.3 Results and Disscussion

Soluble PPEs with symmetric linear chains[18,19] **(LPPE**, Scheme 1) and one-side insulated chains[19–21] (**CPPE**, Scheme 1) were prepared by Sonogashira coupling reactions,[22–24] giving molecular weights of Mn = 5.2×10^4 and Mw = 6.2×10^4 (**LPPE**) and Mn = 1.3×10^4 and Mw = 2.3×10^4 (**CPPE**). The optical transitions of the polymers were recorded in THF as a solvent with an optical path length of 1 cm, or in pristine solid films coated onto quartz substrates. Every spectrum was recorded after attaining thermal stabilization within 0.1 K. The mismatch between the linear thermal expansion coefficients of THF and fused quartz was less than ~8×10^{-4} K^{-1},[25,26] leading to a negligible change in the concentration of the polymers. The presence of isosbestic points in the temperature-induced spectral change of **LPPE** (Figure 1) also indicated that there were negligible effects fromthermal expansion and/or aggregate precipitation on the total concentration of the chromophores. The electronically-conjugated system along the PPE chains

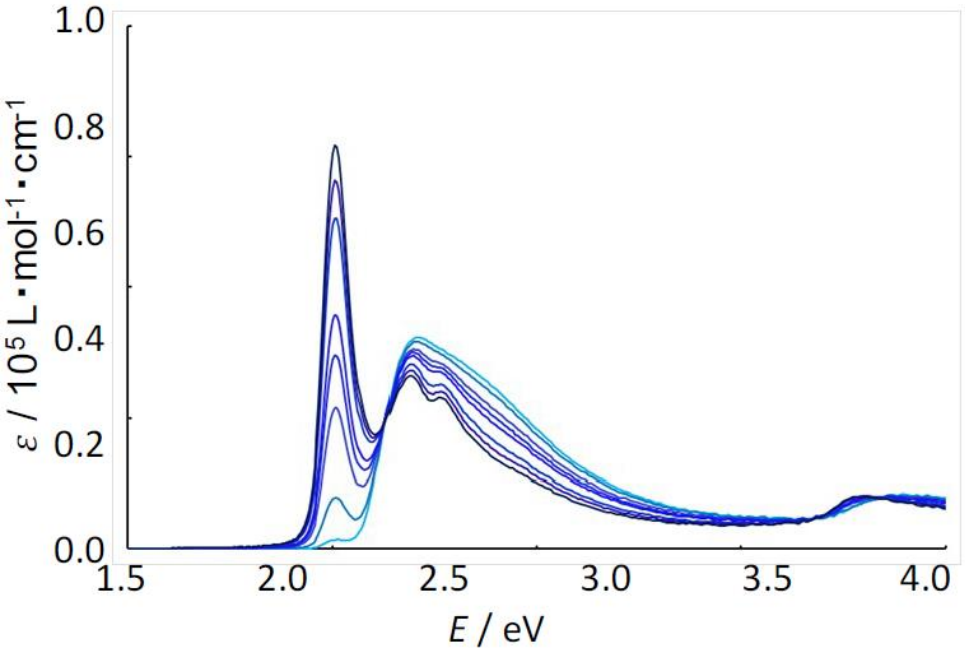

Figure 1. Electronic absorption spectra of **LPPE** in THF (c = 2.1×10^{-5} M) at a variety of temperatures varying from 233 to 253 K.

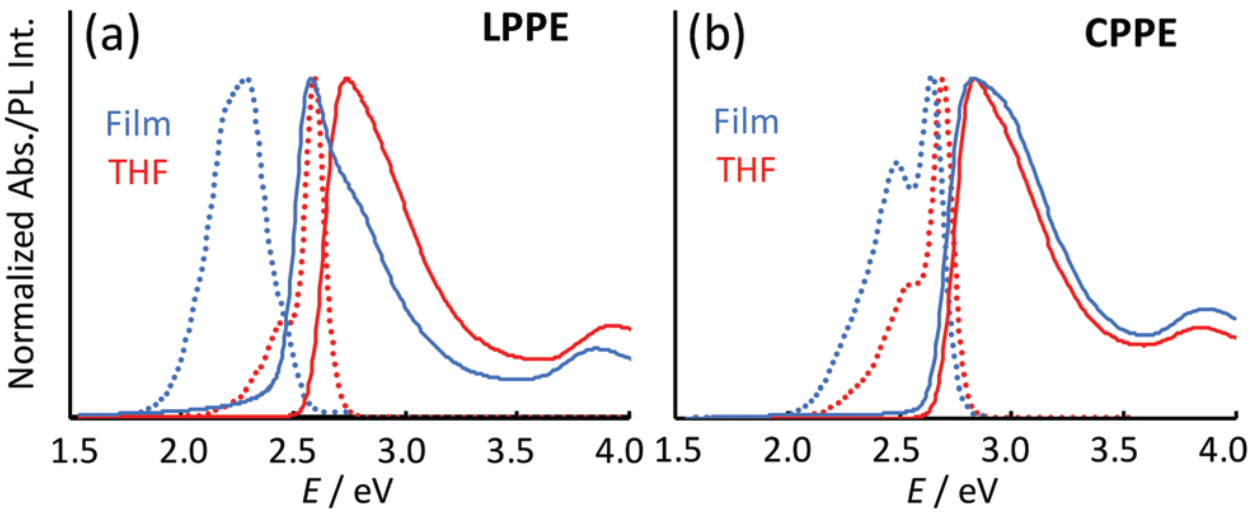

Figure 2 Electronic absorption spectra (solid lines) and fluorescence spectra (dotted lines) of (a) **LPPE** and (b) **CPPE** in THF (c = 2.1×10^{-5} M; base mol unit) (red) together with those of spin-cast films (blue) from $CHCl_3$ solutions of the corresponding polymers (λex = 420 nm).

exhibits a strong electronic transition dipole at 2.8 eV. The spectra are shown in Figure 2 for **LPPE** and **CPPE**, both in diluted solutions and in the condensed phases. In solution, both of the polymers **LPPE** and **CPPE** exhibited very similar absorption profiles at room temperature. The calculated molar extinction coefficients at the maxima were 2.8×10^4 and 2.2×10^4 dm^3 mol^{-1} cm^{-1} for **LPPE** and **CPPE**, respectively, so the values are almost competitive. A weak vibronic feature in the spectra of **CPPE** suggests configurational confinement by the interference of cyclic side chains in **CPPE**.[27,28] In order to investigate the rod like transition as well as the aggregation, low temperature absorption and emission experiments were performed.[29](Figure 3) An initial decrease in the temperature led to a hyperchromic shift with a small red shift in the absorption maxima of both polymers that can be attributed to the planarization of the π-backbone which eventually increases the effective conjugation length, as well as the absorption cross section. However, further deceasing the temperature caused an emergence of a red-shifted sharp absorption band at 2.5 eV along with a vibronic feature in the absorption profile for **LPPE**, whereas **CPPE** showed only a

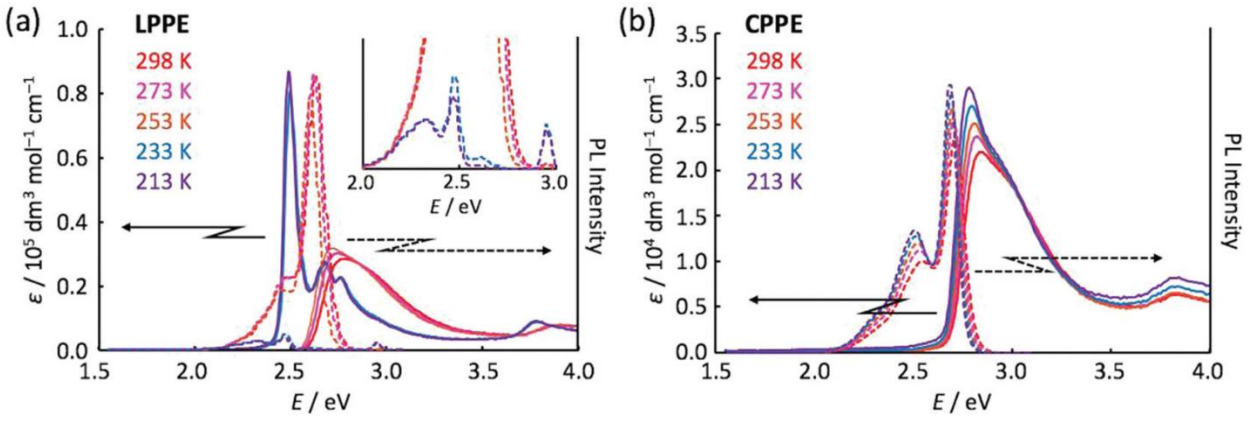

Figure 3. Electronic absorption spectra (solid lines) and fluorescence spectra (dotted lines) of (a) **LPPE** in THF (c = 2.1 × 10^{-5} M; base mol unit) and (b) **CPPE** in THF (c = 1.1 × 10^{-5} M; base mol unit) at various temperatures (lex = 420 nm). Molar extinction coefficients were calibrated against base mol units of the corresponding monomers. The inset in (a) shows an enlarged view of the fluorescence spectra recorded for **LPPE**. The observed apparent emission peak at 2.9 eV for **LPPE** below 233 K is due to the scattering of excitation light which is the sign of aggregate formation.

hyperchromic shift. The vibronic features could be assigned to the 0→0 (<0' |0>) and 0→1 (<1'|0>) transitions observed around 2.5 and 2.7 eV, respectively. The energy levels of the ground and the first excited states of the conjugated π-electron system are presumed to have displacements (*d*) in the nuclear coordinates for the energy minima of both states. Assuming harmonic vibrational oscillations with the base frequency of ω_0, the relative ratio of the first and second vibronic peak strengths can be parameterized by the Huang–Rhys parameter (*S*) as,

$$S = \frac{d^2 m^* \omega_0}{2\hbar}$$

where m^* and $\hbar$ are the effective mass of an electron and Dirac's constant, respectively.[30–33] S can be derived easily and experimentally by,

$$S = \frac{I_{0\to1}}{I_{0\to0}}$$

where $I_{0\text{-}0}$ and $I_{0\text{-}1}$ are the intensities of the 0-0 and 0-1 transitions. The parameter *S* for **LPPE** was estimated to be 0.33 for **LPPE** below 230 K, which is less than half of the values observed in the ordered condensation of P3HT[34] and PPV.[35] The strong exciton-coupled band at low temperature originates from the π-stacking of the available conjugated backbone of **LPPE** with a small change of *d* in its excited state, while insulation restricts the π-stacking[27,28,36] of the **CPPE** backbone.

The narrow red-shifted band of **LPPE** is also a clear signature of well-ordered J-type aggregates; this is the cause of the extremely small value of *S* for **LPPE**. In contrast to the sharp spectral change of **LPPE** upon cooling, only a gradual bathochromic shift was observed for **LPPE** upon addition of a poor solvent (methanol, Figure 4). Fluorescence of **LPPE** was quenched significantly in this solvent mixture as the ratio of poor solvent increased, clearly suggesting the

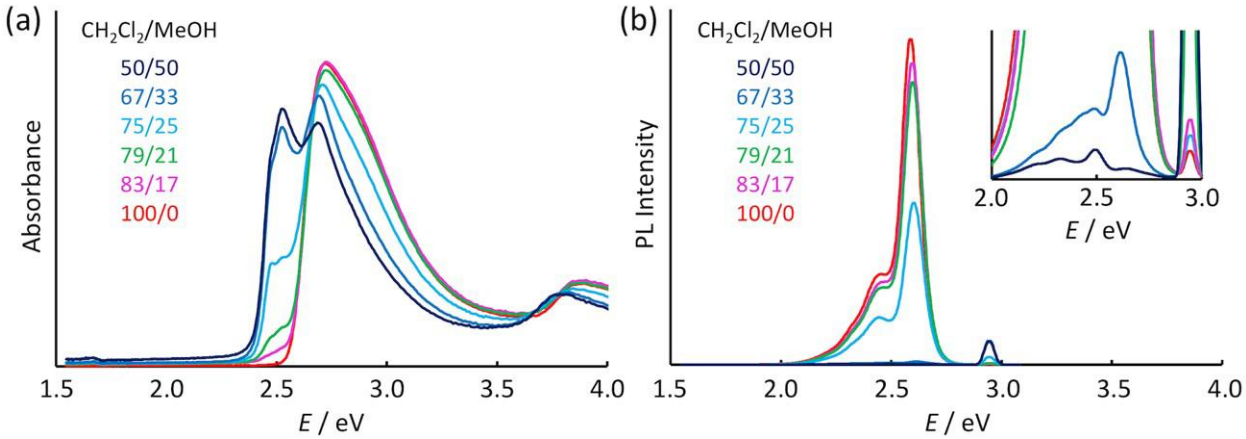

Figure 4. (a) Electronic absorption spectra of **LPPE** in CH_2Cl_2/MeOH mixtures (c = 2.5×10^{-5} M). (b) Fluorescence spectra of **LPPE** in CH_2Cl_2/MeOH mixtures (c = 2.5×10^{-5} M) upon excitation at 420 nm. Superimposed figure represents an enlarged view at the range from 2.0–3.0 eV.

aggregation of **LPPE** chains (Figure 4b). The extent of aggregation of **CPPE** upon addition of methanol is not apparent in the absorption spectra (Figure 5a) but is clear from the fluorescence quenching (Figure 5b). The aggregation of the condensed phase was also monitored via thin film absorption at room temperature. The condensed phase of **LPPE** showed a red-shifted absorption compared to the solution at room temperature, and the broad absorption points towards the formation of random aggregates unlike the behavior in solution at low temperature. On the other hand, the absence of a clear bathochromic shift in the absorption maxima indicates that the π–π interaction was eliminated in the aggregate of **CPPE** even in the condensed phase. The contrasting spectral changes of **LPPE** upon cooling to those in mixed solvent/solid films clearly suggests a rod-like transition of isolated **LPPE** chains at the low temperature.

Furthermore, these rod-like structures of **LPPE** facilitate the formation of ordered J-type aggregates at low temperature, while the transition is incomplete in the mixed solvents and in the condensed phase. The molecular weight of the polymers is generally a primary factor that affects

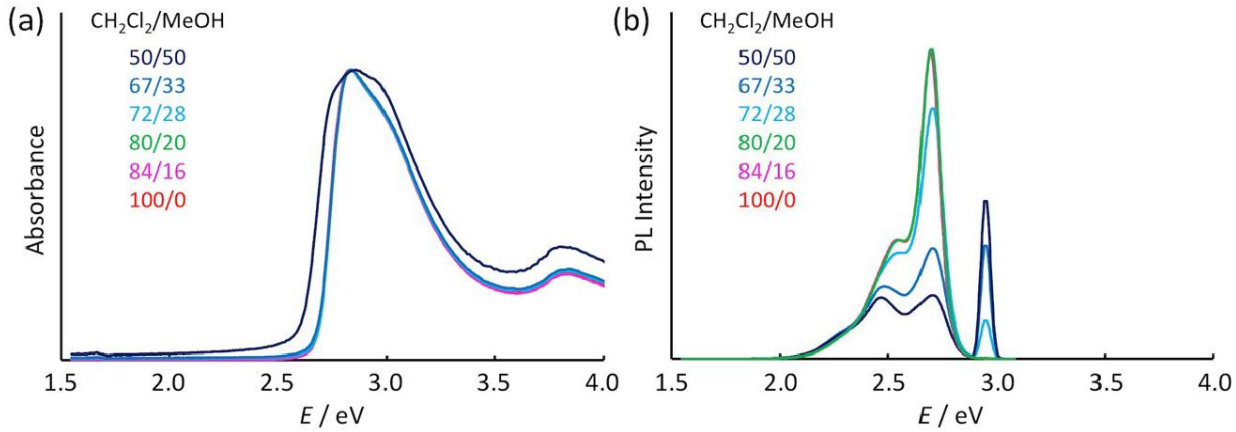

Figure 5. (a) Electronic absorption spectra of **CPPE** in CH_2Cl_2/MeOH mixtures (c = 2.2×10^{-5} M). (b) Fluorescence spectra of **CPPE** in CH_2Cl_2/MeOH mixtures (c = 2.2×10^{-5} M) upon excitation at 420 nm. Superimposed figure represents an enlarged view at the range from 2.0–3.0 eV.

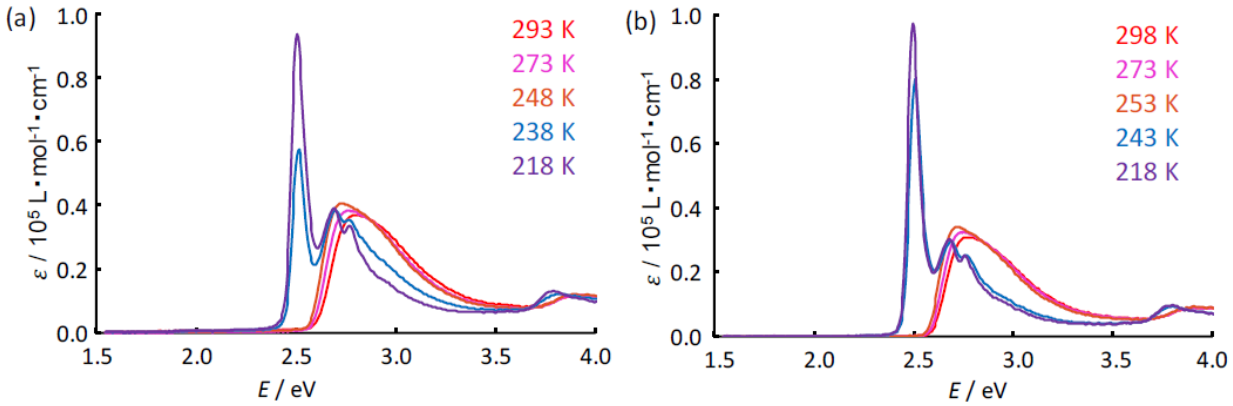

Figure 6. Electronic absorption (solid line) of **LPPE** in THF (a) (Mw = 9.1×10^3, c = 1.0×10^{-5} M; base mol unit) and (b) (Mw = 6.2×10^4, c = 1.1×10^{-5} M; base mol unit) at various temperature.

the aggregation of polymers. Although both the **LPPE** and the **CPPE** show high enough solubility in the solvents used, the former, with its higher molecular weight and rigidity, is presumed to be sensitive to molecular weight in its aggregation behavior. To address the effect of molecular weight, the temperature dependent spectral changes of **LPPE** (Figure 6) was traced, and found almost identical spectral changes with a small shift in the aggregation temperature (233 K - 228 K). This implies that the impact of molecular weight is limited for the aggregation of both **LPPE** and **CPPE**. Solution-state fluorescence spectra revealed that both of the polymers are strongly emissive in the non-aggregated state. Similar to the absorption, a small increase in emission intensity with more structural features was observed in the spectra upon cooling. Below 253 K, a sudden quenching with a bathochromic shift in fluorescence was observed for **LPPE** due to aggregate formation. Interestingly, these aggregates exhibited rare mirror imaged emission spectra with an ultralow Stokes shift (161 cm^{-1}) compared to the non-aggregated polymer, further confirming the formation of well-defined J-type aggregates (Figure 3 and inset).[34]

On the contrary, a concomitant increase in fluorescence intensity was observed for **CPPE** upon cooling, while the Stokes shift (867 cm^{-1}) remained unchanged, suggesting no aggregation. The film of **LPPE** exhibited quenched, non-structured and red-shifted fluorescence with a large Stokes shift (2349 cm^{-1}), due to the formation of disordered/random aggregates in the film state at room temperature (Figure 2a). On the other hand, small bathochromic shifts for the film of **CPPE** on structured fluorescence spectra was observed, originating from the rigidification of the polymer backbone in the solid state. The formation of the highly defined J-aggregates suppressed the energetic divergence of the vibrionic states, leading to an ultralow Stokes shift. From the absorption spectra of **LPPE** and **CPPE**, the oscillator strengths (*f*) and full width at half maxima (FWHM) of the major optical transition band in each polymer were extracted by numerical integration of the extinction coefficient from 300 to 600 nm. The temperature dependence of the oscillator strength f is shown in Figure 7a. Initially a gradual decrease in f was observed for both polymers upon cooling, indicating a decrease in the homogeneous energetic disorder. The apparent discontinuity in both *f* and FWHM for **LPPE** (Figure 7b) around 230 K clearly suggests a phase transition for the polymer backbone due to its aggregation, whereas **CPPE** showed continuous changes across the whole temperature range. The average conjugation length (*n*) in the backbone-conjugated polymers has often been discussed in terms of the maximum energy or optical band gap of the characteristic electronic transition bands.[37,38] However, the total transition dipole, and hence oscillator strength, is the primary choice for a quantitative discussion of the total number of monomer units (*N*) contributing to conjugated electronic systems.

Here the author discuss the segmental relaxation[39,40] of **LPPE** and **CPPE** as a function of temperature. Figure 7a plots the values of *f* against T^{-1}. The gradual increase in *f* upon cooling

clearly suggests an increase in N for both of the polymers. The free energy change ($\Delta\mu$) in the segmental relaxation is estimated from the Arrhenius model (Figure 7 and Figure 8)[6,7] using the least squares fit for f with the following equation,

$$\frac{f(T) - f_{LT}}{f_{LT}} = Aexp\left(-\frac{\Delta\mu}{kT}\right)$$

where f_{LT} is the oscillator strength of **LPPE**/**CPPE** at the lowest temperature. Eqn. (3) gave an excellent linear fit for **LPPE**. However, non-Arrhenius behavior was observed for **CPPE** (Figure 8). It should be noted that the oxydecyloxy chain-strapped monomers have planar chirality[41] (Figure 9), suggesting a considerable increase in $\Delta\mu$ upon cooling via stepwise segmental relaxation at isotactic (RR/SS) or syndiotactic (RS) sequences at the chain end41 and/or interference of the cyclic side chains depending on the sequence (RRR/RRS/RSR) with different rotational barrier heights. The latter is the cause of the non-Arrhenius type segmental relaxation in **CPPE**. The derived value of $\Delta\mu$ is 52 meV for **LPPE**. The rotational barrier of the model compound diphenylacetylene has been predicted to be 18 meV which is much lower than $\Delta\mu$,[42]

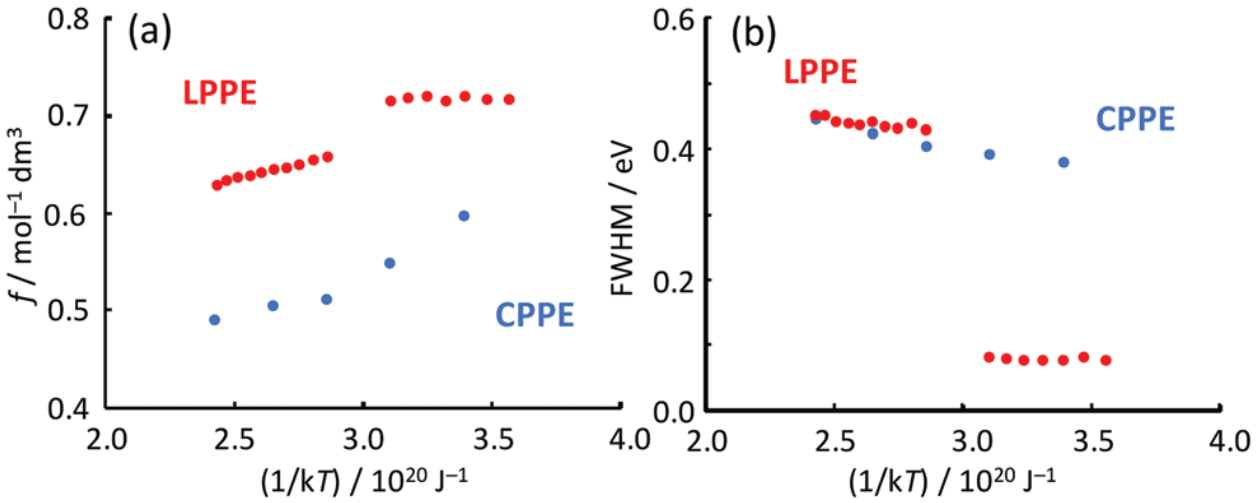

Figure 7. Temperature dependence of oscillator strength (estimated by numerical integration of electronic absorption over 2 to 4 eV) and (b) FWHM of the optical transition band of LPPE (red) and CPPE (blue).

suggesting the key role of the rotational motion of the **LPPE** chain in determining *N* and hence *n*.[43]

Within the sequence showing a gradual elongation of the segment with an increase of *n* upon cooling, the rod-like chain of **LPPE** has a steep change in both *f* and FWHM for its characteristic absorption. In particular, the FWHM value of **LPPE** drops from 480 to 74 meV upon cooling from 298 to 243 K, suggesting that ultralow energetic disorder has been realized in the electronically-conjugated system of **LPPE**. To date the minimum energetic disorder reported for PPE is 94 meV for the PPE with bis[s-(+)-3,7-dimethyloctyl] side chains.[44] An extremely small energetic disorder of the conjugated backbones was also realized in the rod-like helical polysilanes[45] with the smallest FWHM of 60 meV.[46]

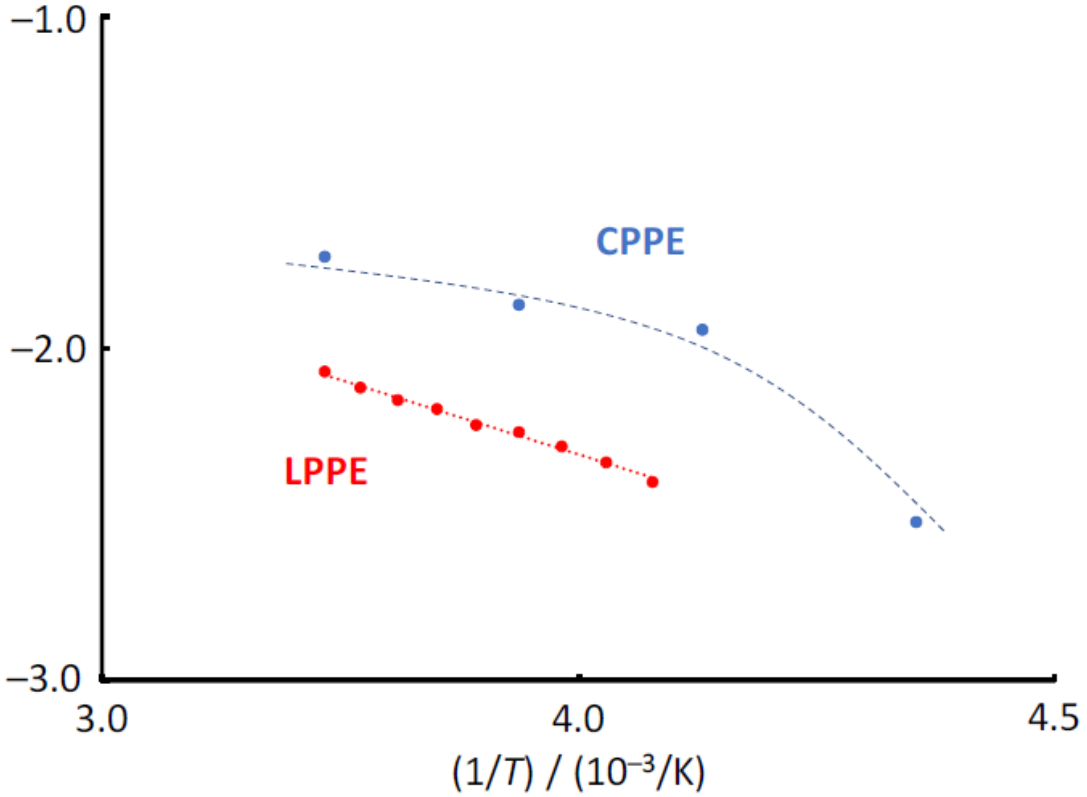

Figure 8. Temperature dependence of oscillator strength. Red-dotted and blue dashed fitting lines are given by the least square method for **LPPE**, and by visual guide for **CPPE**, respectively.

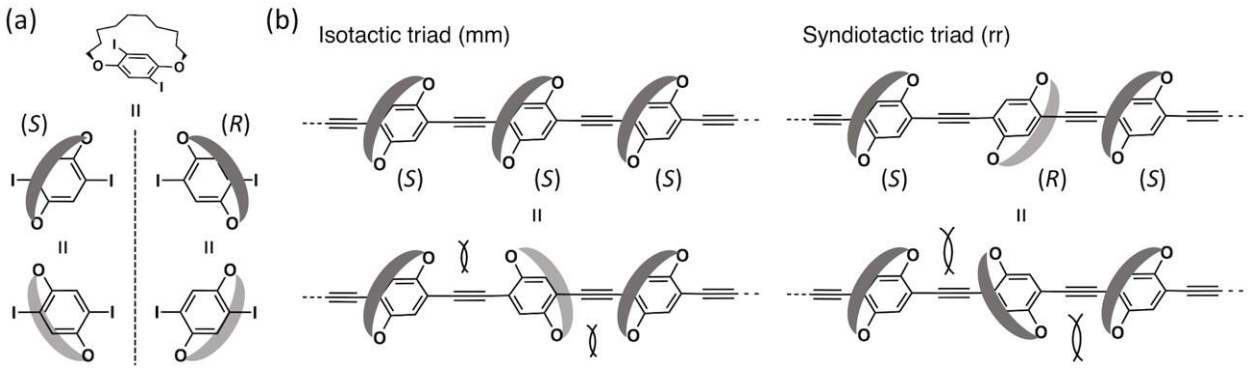

Figure 9. Schematic illustration of (a) stereoisomers of oxydodecyloxy chain-strapped monomers and (b) examples of tacticity for triad.

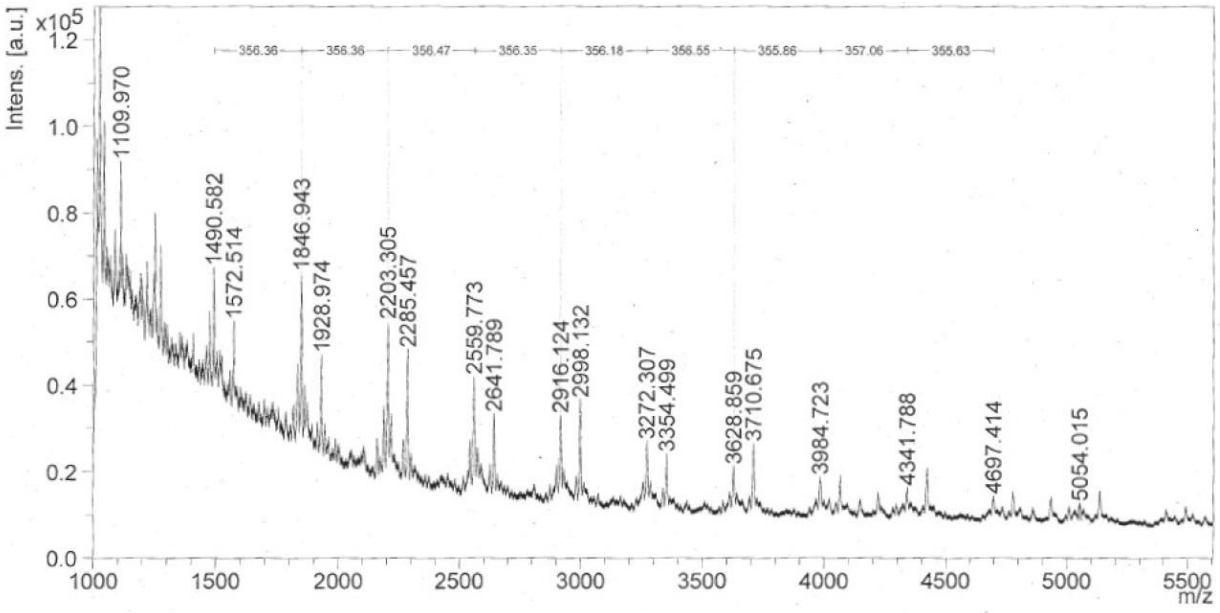

Figure 10. MALDI-TOF mass spectra of **LPPE**.

1.4 Conclusion

bThe present results indicate that the author can achieve a more ordered backbone configuration of PPE with simple substituents instead of chiral substituents that restrict the free rotation of the backbones. The *q* value of PPE chains was reported as ~30 nm in diluted solutions at room temperature.[47] From the molecular weight of **LPPE** (determined using polystyrene (PS) as a standard), the gyration radius of the polymer was estimated as ~8 nm which is much shorter than the *q* value of PPE.[48,49] Indeed, an absolute molecular weight of **LPPE** was determined by matrix assisted laser desorption ionization coupled to time of flight (MALDI-TOF) mass spectrometry (Figure 10), and it showed a striking agreement with the chain length of the polymer. Even upon cooling, the increase in *f* (and hence, *N*) of **LPPE** was less than 20%, which suggests that the chain configuration of LPPE is rod-like at room temperature. The $\Delta\mu$ value estimated herein is comparable to the thermal energy of the PPE backbone; this is consistent with a landscape in which ‘‘twisting’’ of the backbone is predominant in determining the electronic-conjugation length along a PPE backbone, although the shape of the chain is already rod-like at room temperature. The configuration of PPE backbones in solution was studied by electronic absorption spectroscopy and fluorescence spectroscopy of **LPPE** and **CPPE** as soluble PPE derivatives, as a function of temperature. **LPPE** showed a remarkable electronic transition at 2.5 eV below 253 K, exhibiting an ultra-sharp 0-0 transitionband with a FWHM of 74 meV and an ultralow Stokes shift of 161 cm^{-1}.

The fluorescence quenching below 253 K for **LPPE** confirmed the interchain aggregate formation of **LPPE** in that temperature range, whereas **CPPE** showed no quenching of fluorescence. The dramatic change in optical properties suggests an apparent ‘‘electronic conjugation’’ in which there is a steep increase in the persistence length along the backbones,

although the extension of the geometrical *q* value is limited to 20%. Considering the quantitative estimation of free energy in terms of *f* and the absence of a sharp 0-0 band when the aggregates were prepared by the addition of a poor solvent, it appears that the small energetic disorder of the conjugated backbone is only realized below 253 K. This phenomenon can be explained by the suppression of rotational motions of the phenylene units in the PPE backbones via the temperature decrease, which accelerates the chain aggregation. The rod-like transition occurs first, and subsequently the chains assemble into ordered aggregates with the suppression of twisting and rotational motions of the intrachain units.

2.5 Reference

(1) K. C. Lim, C. R. Fincher Jr. and A. J. Heeger, *Phys. Rev. Lett.*, (1983), **50**, 1934–1937.

(2) E. H. Kang and T. L. Choi, *ACS Macro Lett.*, (2013), **2**, 780–784.

(3) F. L. Lee, A. Barati Farimani, K. L. Gu, H. Yan, M. F. Toney, Z. Bao and V. S. Pande, *J. Phys. Chem. Lett.*, (2017), **8**, 5479–5486.

(4) I. Roy and S. Hazra, *RSC Adv.*, (2015), **5**, 665–675.

(5) X.-B. Liu, Y.-F. Zhao, E.-Q. Chen, C. Ye, Z.-H. Shen, X.-H. Fan,S. Z. D. Cheng and Q.-F. Zhou, *Macromolecules*, (2008), **41**, 5223–5229.

(6) P. J. Flory, *J. Chem. Phys.*, (1942), **10**, 51–61.

(7) M. L. Huggins, *J. Phys. Chem.*, (1942), **46**, 151–158.

(8) H. Yamakawa, *J. Chem. Phys.*, (1966), **45**, 2606–2617.

(9) Y. A. Budkov and M. G. Kiselev, *J. Phys.: Condens. Matter*, (2017), **30**, 043001.

(10) D. R. Tree, Y. Wang and K. D. Dorfman, *Phys. Rev. Lett.*, (2013), **110**, 208103.

(11) A. Godt, M. Schulte, H. Zimmermann and G. Jeschke, *Angew. Chem., Int. Ed.*, (2006), **45**, 7560–7564.

(12) B. Kuei and E. D. Gomez, *Soft Matter*, (2017), **13**, 49–67.

(13) T. Sakurai, S. Yoneda, S. Sakaguchi, K. Kato, M. Takata and S. Seki, *Macromolecules*, (2017), **50**, 9265–9275.

(14) P. A. Pincus, G. Rossi and M. E. Cates, *Europhys. Lett.*, (1987), **4**, 41–46.

(15) J.-L. Bredas, D. Beljonne, V. Coropceanu and J. Cornil, *Chem. Rev.*, (2004), **104**, 4971–5003.

(16) D. L. Cheung and A. Troisi, J. Phys. Chem. C, (2010), **114**, 20479–20488.

(17) U. H. F. Bunz, *Chem. Rev.*, (2000), **100**, 1605–1644.

(18) U. H. F. Bunz, *Macromol. Rapid Commun.*, (2009), **30**, 772–805.

(19) J. Huber and U. Scherf, *Macromol. Rapid Commun.*, (1994), **15**, 897–902.

(20) D. K. Fu, B. Xu and T. M. Swager, *Tetrahedron*, (1997), **53**, 15487–15494.

(21) B. McDearmon, E. Lim, I.-H. Lee, L. M. Kozycz, K. O'Hara, P. I. Robledo, N. R. Venkatesan, M. L. Chabinyc and C. J. Hawker, *Macromolecules*, (2018), **51**, 2580–2590.

(22) K. Sanechika, T. Yamamoto and A. Yamamoto, *Bull. Chem. Soc. Jpn.*, (1984), **57**, 752–755.

(23) S. Kang, A. D. Todd, A. Paul, S. Y. Lee and C. W. Bielawski, *Macromolecules*, (2018), **51**, 5972–5978.

(24) M. Su, N. Liu, Q. Wang, H. Wang, J. Yin and Z.-Q. Wu, *Macromolecules*, (2016), **49**, 110–119.

(25) K. Sugiyasu, Y. Honsho, R. M. Harrison, A. Sato, T. Yasuda, S. Seki and M. Takeuchi, *J. Am. Chem. Soc.*, (2010), **132**, 14754–14756.

(26) J. Terao, A. Wadahama, A. Matono, T. Tada, S. Watanabe, S. Seki, T. Fujihara and Y. Tsuji, *Nat. Commun.*, (2013), **4**, 1691.

(27) O.Kiyohara, P. J. D'Arcy and G.C. Benson, *Can. J. Chem.*, (1978), **56**, 2803.

(28) J. Oishi and T. Kimura, *Metrologia*, (1969), **5**, 50.

(29) S. Seki, Y. Kunimi, K. Nishida, Y. Yoshida and S. Tagawa, *J. Phys. Chem. B*, (2001), **105**, 900–904.

(30) K. Huang and A. Rhys, *Proc. R. Soc. A*, (1950), **204**, 406–423.

(31) Z. Shuai, J.-L. Bredas and W. P. Su, *Chem. Phys. Lett.*, (1994), **228**, 301–306.

(32) J. W. Blatchford, S. W. Jessen, L. B. Lin, T. L. Gustafson, D. K. Fu, H. L. Wang, T. M. Swager, A. G. MacDiarmid and A. J. Epstein, *Phys. Rev. B: Condens. Matter Mater. Phys.*, (1996), **54**, 9180–9189.

(33) Y. Motomura, Y. Hattori, T. Sakurai, S. Ghosh and S. Seki, *Macromolecules*, (2019), **52**, 4916–4925.

(34) F. C. Spano and C. Silva, *Annu. Rev. Phys. Chem.*, (2014), **65**, 477–500.

(35) A. Ko¨hler, S. T. Hoffmann and H. Bassler, *J. Am. Chem. Soc.*, (2012), **134**, 11594–11601.

(36) C. Pan, C. Zhao, M. Takeuchi and K. Sugiyasu, *Chem. – Asian J.*, (2015), **10**, 1820–1835.

(37) C. Pan, K. Sugiyasu, Y. Wakayama, A. Sato and M. Takeuchi, *Angew. Chem.*, (2013), **52**, 10775–10779.

(38) S. Seki, Y. Yoshida and T. Tagawa, *Macromolecules*, (1999), **32**, 1080–1086.

(39) S. Seki, Y. Koizumi, T. Kawaguchi, H. Habara and S. Tagawa, *J. Am. Chem. Soc.*, (2004), **126**, 3521–3528.

(40) S. Seki, Y. Matsui, Y. Yoshida, S. Tagawa, J. R. Koe and M. Fujiki, *J. Phys. Chem. B*, (2002), **106**, 6849–6852.

(41) K. Kanda, R. Hamanaka, K. Endo and T. Shibata, *Tetrahedron*, (2012), **68**, 1407–1416.

(42) R. Fiesel, J. Huber, U. Apel, V. Enkelmann, R. Hentschke, U. Scherf and K. Cabrera, *Macromol. Chem. Phys.*, (1997), **198**, 2623–2650.

(43) J. Kim and T. M. Swager, *Nature*, (2001), **411**, 1030–1034.

(44) J. M. Seminario, A. G. Zacarias and J. M. Tour, *J. Am. Chem. Soc.*, (1998), **120**, 3970–3974.

(45) R. Fiesel, C. E. Halkyard, M. E. Rampey, L. Kloppenburg, S. L. Studer-Martinez, U. Scherf and U. H. F. Bunz, *Macromol. Rapid Commun.*, (1999), **20**, 107–111.

(46) S. Seki and S. Tagawa, *Polym. J.*, (2007), **39**, 277–293.

(47) M. Fujiki, *J. Am. Chem. Soc.*, (2000), **122**, 3336–3343.

(48) J. H. Moon and T. M. Swager, *Macromolecules*, (2002), **35**, 6086–6089.

(49) J.-M. Guenet, *Phys. Rev. Lett.*, (1987), **58**, 1531–1532.

Chapter 2

Impact of Asymmetric Alkyl–Fluoroalkyl Side Chains of Soluble Polyacetylenes on Aggregation Phase

2.1 Introduction

Polyacetylenes (PAs), the oldest and simplest conjugated backbones were synthesized in 1971 by Shirakawa and co-workers.[1,2] As seen in the giant leap in electric conductivity upon chemical doping to PAs,[3] the π–conjugated backbones have been recognized as an efficient platforms for the charge carrier transporting pathways, pioneering to the first 'flexible' electronic materials based on macromolecular systems.

Electronic nature of the conjugated backbone was been also of interests because of their unique electronic systems of charged states. For instance, a positive charge on the backbone shows strong coupling with the vibrational motion of the backbones, gaining solitonic states reflecting a symmetric nature of wave functions of the charge states.[4]

The energetic status of such charged species were also well considered with very sophisticated theoretical approaches started from well–known Su–Schrieffer–Heeger Hamiltonian.[5] The resulted formulations gave eventually as a transition successful interpretation to the delocalization of charge carriers on to conjugated systems, and hence the high electric conductivity upon doping. The asymmetric nature of the wave functions thus depends strongly on the degree of ordering of the conjugated backbones of polyacetylenes. Unfortunately, in contrast to the initial great success

of the chemical doping, the precise control of backbone configuration had not been addressed because of their extremely low solubility against any solvent.

The Ziegler−Natta catalyst had been one of the primary choices for the polymerization of acetylenes,[1−3] resulting in PAs with high molecular weight, high melting point, and controlled morphology in their condensed phase.[6−9] However, this catalyst often encapsulated into polymer chains; thus, it was difficult to remove it from the final product.[7,8] Choi et al. succeeded in synthesizing soluble substituted PAs by living cyclopolymerization of 1,6-heptadiyne derivatives via the olefin metathesis reaction promoted by the third-generation Grubbs catalyst.[10−16] This sophisticated living cyclopolymerization enabled us to produce selectively conjugated polymers composed of 5-membered-ring structures with excellent control over molecular weight and polydispersity index. The polymerization protocol has been extended into polymerization of poly(cyclopentenylene-vinylene) (PCPV), showing the clear coil-to-rod transition of its conjugated backbones by simple aging upon light exposure.[11,12] Unfortunately, the rodlike chain is energetically favored but not chemically stable in good solvents of the polymers such as $CHCl_3$, and the conjugated backbones are going to degrade via an attack of radical species.[17] To utilize the rodlike form of the polymer backbone where excess charges are delocalized, it has been presumed to fix the energetically stable rodlike configurations rapidly by aggregation in the condensed phases.[18−20] The ordered backbone configuration of conjugated macromolecular systems often leads to stable molecular packing (crystalline domains) in the solid states, suppressing simultaneous backbone degradation upon thermal stimuli.[21,22] Nevertheless, in the solid state, polymers with high crystallinity can be folded without hampering the charge transporting property because of the large free volumes and intercrystallite disordered phases, which is considered as a major advantage of polymer conductors/semiconductors in practical devices.[23,24] An effective

strategy to facilitate the ordered solid-state structure of the polymeric materials is the introduction of unsymmetrical side chains into the system.[25,26] Asymmetric van der Waals interactions lead to simultaneous ordering of the backbone configuration as well as aggregated structures with asymmetric spatial alignment of alkyl side chains.[27] Fluoroalkyl substituents are classical but representative molecular motifs exhibiting strong interchain interactions in macromolecular systems.[28,29] Even for the small molecular systems, solid-state ordering can be promoted by the combination of fluoroalkyl and alkyl chains.[30–33] The immiscible nature of superhydrophobic/ hydrophobic segments works as the major driving force to form fluoroalkyl/alkyl nanodomains.[34,35] In view of practical device fabrication, the aggregation dynamics of the conjugated polymer chains in precursor solution is the fundamental and key factor to obtain the desired thin film morphology of polymer semiconductor films.[36–38] Herein, we report for the first time that the combination of unsymmertical substitution and the introduction of fluoroalkyl side chains allows us to control backbone configurations as well as aggregation of PAs in solutions and to transfer them into condensed phases.

Scheme 1. Synthetic Scheme of Poly(cyclopentenylene-vinylene) Derivatives **C6−C6**, **C6−C2F4**, **C6−C1F5**, and **C2F4−C2F4**

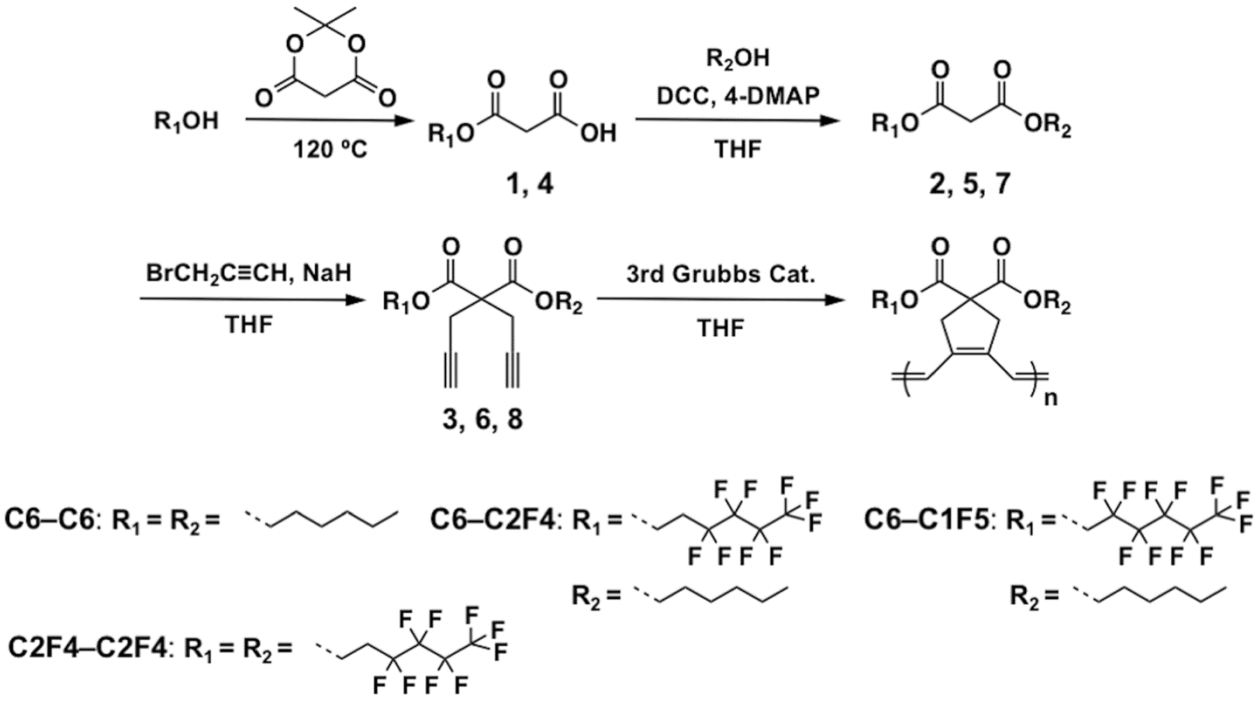

2.2 Experimental Section

Unless otherwise noted, all commercial reagents were purchased from Wako Pure Chemical Industries Ltd., Tokyo Chemical Industry Co. Ltd. and Sigma-Aldrich Co. and used as received. The detailed synthetic schemes are described in the supplementary material. Column chromatography was performed on Silica Gel 60N (spherical, neutral) from Kanto Chemicals. Molecular weights of polymers were determined by size exclusion chromatography (SEC) with polystyrene standards. SEC analysis was performed on HITACHI model L-2130, L-2455, L-2530 chromatography instruments with Shodex KF-804L/KF-805L columns using THF as an eluent at a flow rate of 1 mL min^{-1} at room temperature. A refractive index detector and multi-wavelength photodiode array detector were used for detecting the elution peaks. Electronic absorption spectra

were recorded on a JASCO model V-570 spectrometer with a Unisoku model CoolSpeK UV USP-203 temperature controller.

^{1}H-NMR spectra were recorded by a JEOL model JNM-AL400 spectrometer. Chemical shifts of ^{1}H-NMR spectra are determined relative to internal tetramethylsilane (TMS) standard (δ), and are given in parts per million (ppm). ^{19}F-NMR spectrum of **C6-C2F4** was obtained with a JEOL model JNM-ECS400 spectrometer and the chemical shifts was determined relative to external ethyl trifluoroacetate (δ = -78.00). ^{19}F-NMR spectra and DPFGSE NOE spectra were recorded by a JEOL model JNM-ECZ500R/S1 spectrometer. Chemical shifts of **C6-C1F5** of ^{19}F-NMR spectra were determined relative to external sodium trifluoromethanesulfonate (δ = -78.80). The selective 180° pulses in the DPFGSE NOE were 20 ms long Gaussian pulses. The length of the applied pulsed field gradients (60, 90, and 30 mT/m) was 1 ms.

General polymerization procedure

All the polymers were synthesized in a similar way to the reported procedure of **PCPV** (ref). The monomer was added to a 30 mL Schlenk flask. The flask was purged with nitrogen, and dry THF was added ($[M]_0$ = 0.5 M). The catalyst ([M] / [I] = 25) was added at once under vigorous stirring at 0 ℃ for 1h. The reaction was quenched by excess ethyl vinyl ether, and precipitated by methanol. The dark purple solid was obtained by filtration and dried in vacuum.

C6-C6: The polymer was synthesized according to the literature. [12]

C6-C2F4: ^{1}H-NMR(400 MHz, $CDCl_3$) δ = 0.85 (m, br, 3H), 1.27 (m, br, 6H), 1.64 (m, br, 2H),

2.34-2.60 (m, br, 2H), 3.14-3.42 (m, br, 4H), 4.17 (m, br, 2H), 4.50 (m, br, 2H), 6.23-6.68 (m, br, 2H); ^{19}F-NMR(400 MHz, $CDCl_3$) δ = -128.37 (m, br, 2F), -126.80 (m, br, 2F), -116.22 (m, br, 2F), -83.42 (m, br, 3F)

C6-C1F5: ^{1}H-NMR(400 MHz, C_4D_8O) δ = 0.88 (m, br, 3H), 1.31 (m, br, 6H), 1.63 (m, br, 2H), 3.21-3.45 (m, br, 4H), 4.12 (m, br, 2H), 4.83 (m, br, 2H), 6.34-6.90 (m, br, 2H); ^{19}F-NMR(500 MHz, C_4D_8O) δ = -127.47 (m, br,2F), -124.68 (m, br, 2F), -124.09 (m, br, 2F), -120.68 (m, br, 2F), -82.37 (m, br, 3F)

3-((1H,1H,2H,2H-nonafluorohexyl)oxy)-3-oxopropanoic acid (1): A mixture of 1H,1H,2H,2H-nonafluoro-1-hexanol (2 g, 7.57 mmol) and meldrum's acid (1.31 g, 9.09 mmol) was heated at 120 ℃ under vigorous stirring for 3h. After cooling to room temperature, the product was dried in vacuum to afford compound **1** as a white solid (2.47g, 7.04 mmol, 93%). ^{1}H-NMR(400 MHz, $CDCl_3$) δ = 2.50 (m,2H), 3.46 (s, 2H), 4.47 (t, J = 6.4 Hz, 2H)

Hexyl (1H,1H,2H,2H-nonafluorohexyl) malonate (2): A solution of compound **1** (1.5 g, 4.28 mmol), 1-hexanol (0.53 g, 5.14 mmol), and 4-DMAP (62.3 mg, 0.51 mmol) in dry CH_2Cl_2 (70 mL) was cooled to 0 ℃ under nitrogen atmosphere. DCC (1.06 g, 5.14 mmol) in dry CH_2Cl_2 (10 mL) was added subsequently. After stirring the solution for 1h at 0 ℃, the reaction mixture was warmed to room temperature, stirred overnight. Then, the reaction mixture was evaporated, poured into hexane, and filtered from a white powder. The solution was evaporated and purified by column chromatography on silica gel (ethyl acetate : hexane = 1:9) to afford compound **2** as a colorless oil (1.54 g, 3.55 mmol, 83%). ^{1}H-NMR(400 MHz, $CDCl_3$) δ = 0.87 (t, J = 6.8 Hz, 3H), 1.31 (m,

6H), 1.62 (m, 2H), 2.48 (m, 2H), 3.38 (s, 2H), 4.12 (t, *J* = 6.8 Hz, 2H), 4.44 (t, *J* = 6.6 Hz, 2H)

1-hexyl 3-(1H,1H,2H,2H-nonafluorohexyl) 2,2-di(prop-2-yn-1-yl) malonate (3): Under nitrogen, sodium hydride (0.21 g, 60 wt% in mineral oil, 5.3 mmol) was suspended in dry THF (5 mL) at 0 ℃. Compound **2** (1 g, 2.3 mmol) in dry THF (0.5 mL) was added dropwise to the reaction mixture that was afterwards stirred for 30 min and allowed to warm to room temperature. Then, propargyl bromide (0.63 g, 80% in toluene, 5.3 mmol) was added dropwise and stirred overnight at room temperature. The reaction mixture was quenched with saturated NH_4Cl aqueous solution and stirred for a few minutes. The mixture was extracted by ethyl acetate and the organic layer was dried with Na_2SO_4 and evaporated. The crude product was purified by column chromatography on silica gel (ethyl acetate : hexane = 1:30) to afford compound **3** as a colorless oil (0.63 g, 1.24 mmol, 54%). ^{1}H-NMR(400 MHz, $CDCl_3$) δ = 0.87 (t, J = 7.0 Hz, 3H), 1.30 (m,6H), 1.61 (m, 2H), 2.02 (t, *J* = 2.8 Hz, 2H), 2.46 (m, 2H), 2.99 (d, *J* = 3.2 Hz, 4H), 4.14 (t, *J* = 6.6 Hz, 2H), 4.46 (t, *J* = 6.4 Hz, 2H)

3-oxo-3-((1H,1H,-undecafluorohexyl)oxy) propanoic acid (4): A mixture of 1H,1H-Undecafluoro-1-hexanol (2g, 6.67 mmol) and meldrum's acid (1.15 g, 7.98 mmol) was heated at 120 ℃ under vigorous stirring for 3h. After cooling to room temperature, the product was dried in vacuum to afford compound **4** as a white solid (2.37g, 6.14 mmol, 92%). ^{1}H-NMR(400 MHz, CD_2Cl_2) δ = 3.58 (s, 2H), 4.70 (t, *J* = 13.6 Hz, 2H)

Hexyl (1H,1H-undecafluorohexyl) malonate (5): A solution of compound **4** (1.5 g, 3.88 mmol), 1-hexanol (0.48 g, 4.66 mmol), and 4-DMAP (47.6 mg, 0.39 mmol) in dry CH_2Cl_2 (70 mL) was

cooled to 0 ℃ under nitrogen atmosphere. DCC (0.96 g, 4.66 mmol) in dry CH_2Cl_2 (10 mL) was added subsequently. After stirring the solution for 1h at 0 ℃, the reaction mixture was warmed to room temperature, stirred overnight. Then, the reaction mixture was evaporated, poured into hexane, and filtered from a white powder. The solution was evaporated and purified by column chromatography on silica gel (ethyl acetate : hexane = 1:9) to afford compound **5** as a colorless oil (1.46 g, 3.10 mmol, 80%). ^{1}H-NMR(400 MHz, CD_3Cl) δ = 0.82 (t, *J* = 6.8 Hz, 3H), 1.26 (m, 6H), 1.57 (m, 2H), 3.43 (s, 2H), 4.09 (t, *J* = 6.8 Hz, 2H), 4.59 (t, *J* = 13.6 Hz, 2H)

1-hexyl 3-(1H,1H-undecafluorohexyl) 2,2-di(prop-2-yn-1-yl) malonate (6): Under nitrogen, sodium hydride (0.19 g, 60 wt% in mineral oil, 4.8 mmol) was suspended in dry THF (5 mL) at 0 ℃. Compound **5** (1 g, 2.1 mmol) in dry THF (0.5 mL) was added dropwise to the reaction mixture that was afterwards stirred for 30 min and allowed to warm to room temperature. Then, propargyl bromide (0.57 g, 80% in toluene, 4.8 mmol) was added dropwise and stirred overnight at room temperature. The reaction mixture was quenched with saturated NH_4Cl aqueous solution and stirred for a few minutes. The mixture was extracted by ethyl acetate and the organic layer was dried with Na_2SO_4 and evaporated. The crude product was purified by column chromatography on silica gel (ethyl acetate : hexane = 1:80) to afford compound **6** as a colorless oil (0.49 g, 0.90 mmol, 43%). ^{1}H-NMR(400 MHz, CD_3Cl) δ = 0.87 (t, *J* = 6.8 Hz, 3H), 1.31 (m, 6H), 1.61 (m, 2H), 2.05 (t, *J* = 2.6 Hz, 2H), 3.02 (dd, *J* = 1.4 Hz, 4H), 4.15 (t, *J* = 6.6 Hz, 2H), 4.65 (t, *J* = 13.2 Hz, 2H)

2.3 Results and Discussion

Table 1. Molecular Weights, Polydispersity Indices, Absorption Maxima, and Fitting Results for Vibronic Absorption Bands by Gaussian Functions

entry	M_n [a] (g mol^{-1})	M_w [a] (g mol^{-1})	PDI	λ_{max} (nm)
C6–C6	1.8×10^4	2.0×10^4	1.11	586
C6–C2F4	2.8×10^4	2.9×10^4	1.04	583
C6–C1F5	2.5×10^4	3.4×10^4	1.36	582

	0 → 0		0 → 1		0 → 2		0 → 3	
entry	λ_{max} (FWHM) (eV)	I [b]	λ_{max} (FWHM) (eV)	I [b]	λ_{max} (FWHM) (eV)	I [b]	λ_{max} (FWHM) (eV)	I [b]
C6–C6	0.1064	1	0.1707	0.98	0.1852	0.62	0.1565	0.34
C6–C2F4	0.1086	1	0.1737	1.05	0.1928	0.72	0.1548	0.39
C6–C1F5	0.1091	1	0.1685	0.99	0.2044	0.70	0.1485	0.34

a Determined relative to polystyrene calibration standards. b Relative components of vibronic absorption bands resolved by fitting with Gaussian functions to $I_{0\rightarrow0}$ at 298 K.

Living cyclopolymerization with a third–generation Grubbs catalyst could be successively applied to all the series of monomers designed in the present study to afford corresponding polymers with the high enough molecular weight. Table 1 shows the number and weight average molecular weight of the resulting polymers. A relatively longer chain length was recorded for the polymers with fluorinated alkyl chains, and their polydispersity indices were less than 1.4. Alkyl–symmetric (**C6–C6**) and alkyl–fluoroalkyl asymmetric (**C6–C2F4**, **C6–C1F5**) exhibited sufficient solubility in some representative solvent such as THF, chloroform, dichloromethane, etc. All the polymer could be dissolved in THF for the subsequent spectroscopic analysis.

Figure 1 shows electronic absorption spectra of the series of polymers: **C6-C6**, **C6-C2F4**, and **C6-C1F5** respectively. All the polymers exhibited electronic transitions in the range from 2.0 to

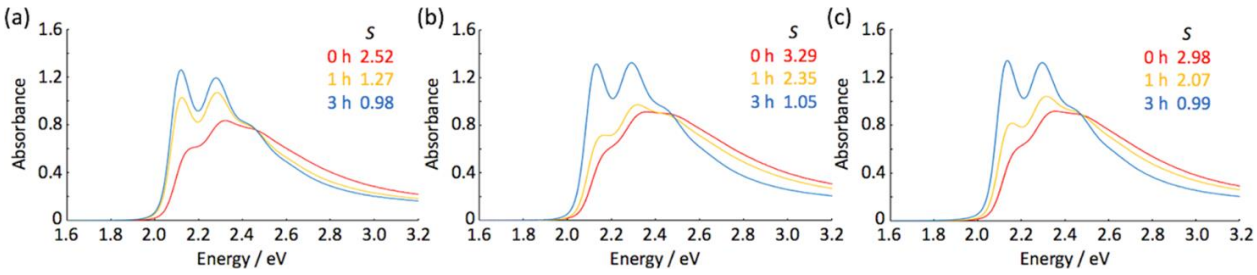

Figure 1. Electronic absorption spectra of (a) **C6−C6** (c = 5.1×10^{-5} M), (b) **C6−C2F4** (c = 8.1×10^{-5} M), and (c) **C6−C1F5** (c = 6.6×10^{-5}M) in THF. All of the spectra were recorded at 0, 1, and 3 h after starting the aging process.

2.8 eV with the clear signature of vibronic states, which can be attributed to the ground to the first excited states of the conjugated π–electron system along the main chain. The vibronic features are importantly remarkable for the transitions assignable to 0→0 (<0' |0>) and 0→1 (<1'|0>) ones observed around 2.1 and around 2.3 eV, respectively. The spectra were monitored at the energy stage of aging by ambient light, where photo–isomerization occurred in the configuration of the conjugated backbones. The aging duration was optimized for each polymer giving maximum absorbance of the lowest energy transition. Further aging by exposure to light caused a significant decrease in the absorbance of the whole spectra.

The representative model for the appearance of vibronic peaks is schematically displayed in Figure 2. The energy levels of ground and the first excited states of the conjugated π–electron system are presumed to have a displacement (d) in the nuclear coordinates for the energy minima of both states. Assuming harmonic vibrational oscillations on the states with the base frequency of ω_0, the relative strength of the first and second vibronic peak can be parameterized by Huang–Rhys parameter (S) as,

$$S = \frac{d^2 m^* \omega_0}{2\hbar}$$

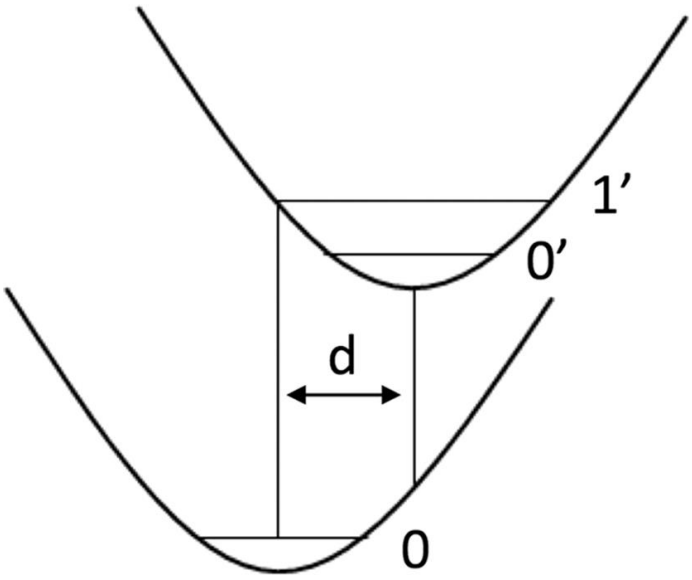

Figure 2. Two electronic states displaced as harmonic oscillators.

where m^* and $\hbar$ are mass of one electron (effective mass is one can consider 1–dimensional electronic band structure with the direct gap) and Dirac’s constant, respectively.[39-45]

All of the polymers exhibited vibronic structures in the absorption spectra (Figure 1) that were deconvoluted and fit by multiple Gaussian functions, consisting of a set of four distinct Gaussian functions. The resulted component of the lowest ($I_{0\rightarrow0}$) and the second lowest ($I_{0\rightarrow1}$) transition energy were used to estimate *S* experimentally,

$$S = \frac{I_{0\rightarrow1}}{I_{0\rightarrow0}}$$

and this analytic protocols were employed for successive spectra of the polymers under variable temperature.

The values of *S* were gradually decreased from around 3.0 to 1.0 with aging for all the polymers. This is suggestive that the aging was successfully worked for all the polymer via photo–isomerization and the global main chain configuration turned from coil to rod-like ones. The

transition observed in **C6-C6** was also reproducible of the precious report by Tae-Lim Choi. [11,12]

To confirm the coil-to-rod transition of the conjugated backbones, decrease of the number of chain segments cooperative to the backbone conjugation (the portions of the units in the disordered structures) was discussed by the change in total transition dipoles in visible range.[46-49] The total transition dipoles (oscillator strength, *f*) were estimated numerically by an integration of the spectra over the regime of 1.65 eV (750 nm) to 2.76 eV (450 nm), where all the vibronic peaks in the inter–band transition has been taken into account.

The aging of **C6-C6**, **C6-C2F4**, and **C6-C1F5** gave a big leap in *f* with about 26% increase. Photoismerization in aging process leads significantly the orientation of the trans–conformers in the backbone and giving rod–like shape of the polymers.

The coil–to–Rod transition is presumed to be advantages to facilitate molecular aggregates into more ordered manner in both solution and condensed phases. To address the aggregation dynamics, electronic absorption spectra was traced under variable temperature. The absorption spectra of **C6-C6** were recorded at the modulated temperature from 298K to 193K before and after aging process (Figure 3a,b). A slight red shift in absorption spectra was observed both before and afterbaging. However, the vibronic structures become sharp particularly after aging. The valueand *S* went down to 0.8, which was the lowest one for the polyacetylenes derivatives and suggestion of highly extended conjugation in these polymers (Figure 3d). In contrast, the full width at half maximum (FWHM) for 0→1 and 0 →0 peaks were almost constant suggesting energetic divergence of the vibronic states was not suppressed enough even in the lowest temperature at 193K. The values of *f* for both before and after aging decreased monotonically upon cooling, implying that as lowering temperature, the thermal vibration of the isolated backbone was more suppressed and became more planar, thus the number of the electrons participating in the conjugated systems was increased

(Figure 3c).

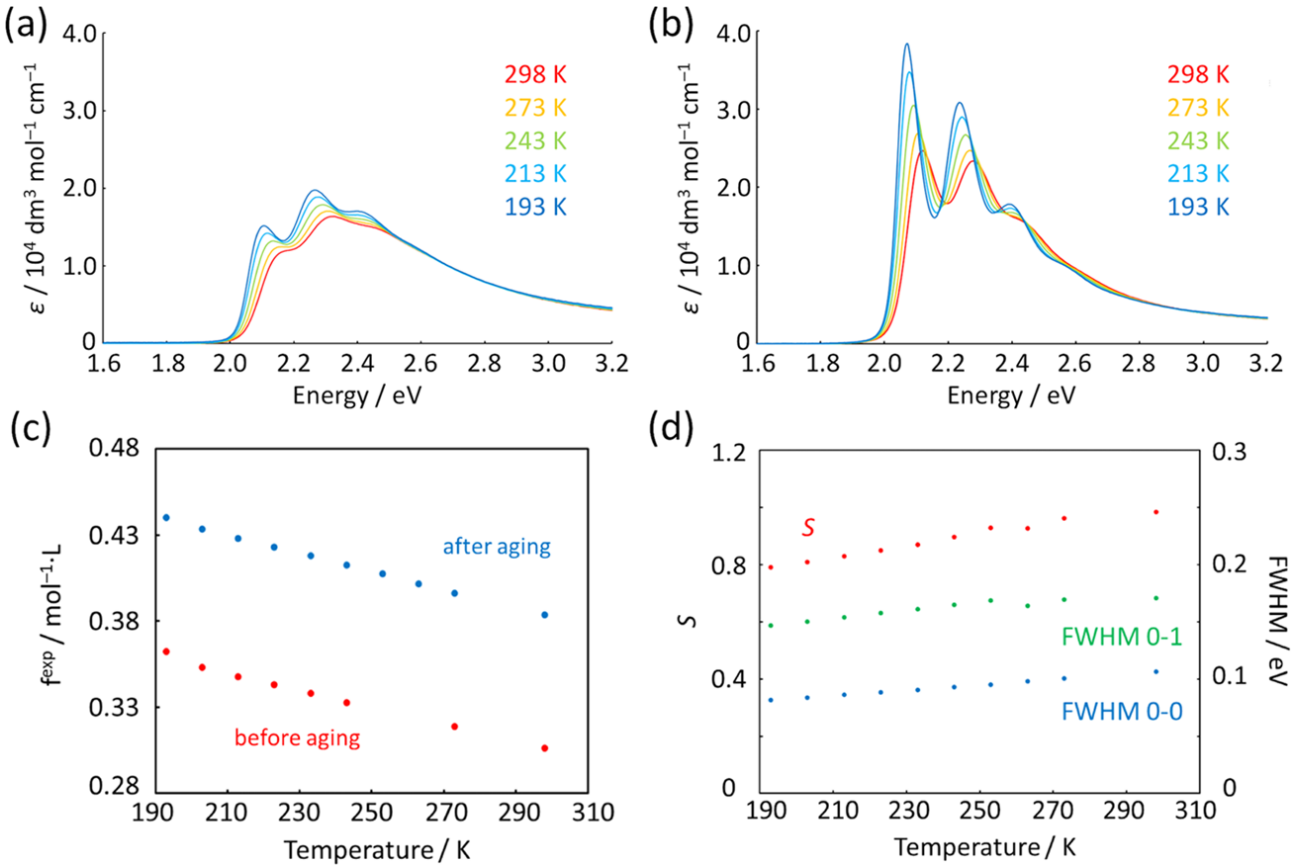

Figure 3. Extinction coefficient of **C6−C6** (c = 5.1×10^{-5} M) (a) before and (b) after aging in THF at various temperatures. (c) Oscillator strength of **C6−C6** before and after aging in THF at various temperatures. (d) The Huang−Rhys factor S (red) and full width at half-maximum (FWHM) of the 0−0 (blue) and the 0−1 (green) vibronic peaks of **C6−C6** in the Gaussian function at various temperatures.

In the case of **C6-C2F4** as shown in Figure 4(a) and 4(b), the change depending on temperature showed a similar behavior with **C6-C6** before aging, while for after aging, the new peak around 1.9 eV clearly appeared below 213K with an isobestic point around 2.1 eV, suggesting an interconversion of two forms of the conjugated backbones. The value of *f* and *S* was plotted against temperature in Figure 4(c) and 4(d). The clear kink points of these curve was seen only for after aging. Temperature dependent spectra of **C6-C1F5** changed in a totally different manner, as shown

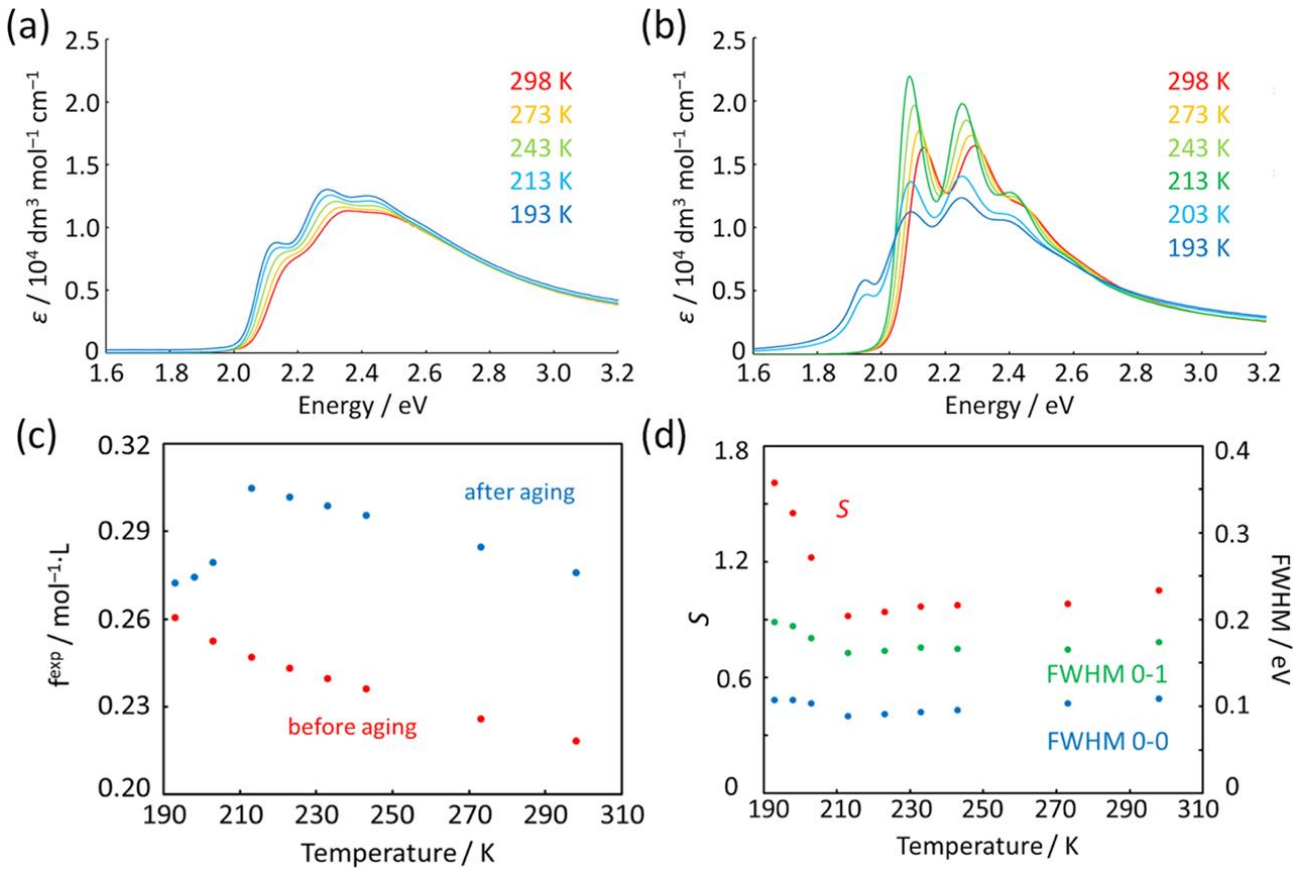

Figure 4. Extinction coefficient of **C6−C2F4** (c = 8.1×10^{-5} M) (a) before and (b) after aging in THF at various temperatures. (c) Oscillator strength of **C6−C2F4** before and after aging in THF at various temperatures. (d) The Huang−Rhys factor S (red) and full width at half-maximum (FWHM) of the 0−0 (blue) and the 0−1 (green) vibronic peaks of **C6−C2F4** in the Gaussian function at various temperatures.

in figure 5(a) and 5(b). For both before and after aging, evident and clear new peak observed in range of 1.8 to 2.0 eV. This new peak was gradually intensified upon cooling with an tic point around 2.1 eV. The value of *f* was also plotted against temperature in Figure 5(c). Unlikely to the case of **C6-C6**, a clear kink of the curve was seen at 220 K and 260K respectively for before and after aging. The decrease in *f* below the kink indicates clearly the correlation of the transition dipole along the conjugated electron systems in the backbone.

The cancellation can be interpreted by the backbone aggregation in the solution even at the diluted conditions, and the well-ordered parallel alignment of the rodlike chains into aggregates contributes significantly to the reduction of the total transition dipoles of the systems.[50] It should also be noted that the spectra did not show any clear signature of the light scattering in the overall range of the spectra (no gradual shift of the baseline, clear observation of isosbestic points), suggesting that the size of the aggregates was smaller than the visible wavelength (Figures 4b and 5b). The observed shift in the temperature at the kink point is also supportive of the formation of the ordered aggregates, where the increase in the inter chain aggregation enthalpy between the rod–like chains after aging facilitates an effective aggregation of the polymers at the higher temperature than that of coil–forms before aging.

In case of the rod–like chains after aging, the appearance of the new peak explicitly consumes both 0→0 and 0→1 transitions with an isobestic point (Figures 4b and 5b). This is suggestive of the simple aggregation of rod–like chains without any conformational change in the backbone constituents. A contrasting change in the value of f with temperature was observed for both **C6−C2F4** and **C6−C1F5** polymers before and after aging (Figures 4c and 5c). For **C6−C1F5**, the former showed a first increase followed by a decrease at 233 K, while the latter showed a monotonic decrease from 273 K. It is rational that the polymer before aging was associated with

the conformational transformation of isolated chains upon cooling from 298 to 223 K.

Considering the dimer model of the conjugated segments in nearby chains in the aggregates, the decrease in the transition dipole can be well interpreted by the formation of J-type aggregates as well from the peak shift.[51] Given the perfect rodlike chains and the stacked aggregates with a phase shift, the overall transition dipoles cancel with each other within the stacked phases due to a small contribution from off-diagonal terms in bimolecular Hamiltonian for excited states, leading to the reduction of the total dipoles. In contrast, the uncanceled dipoles are arranged in line and the

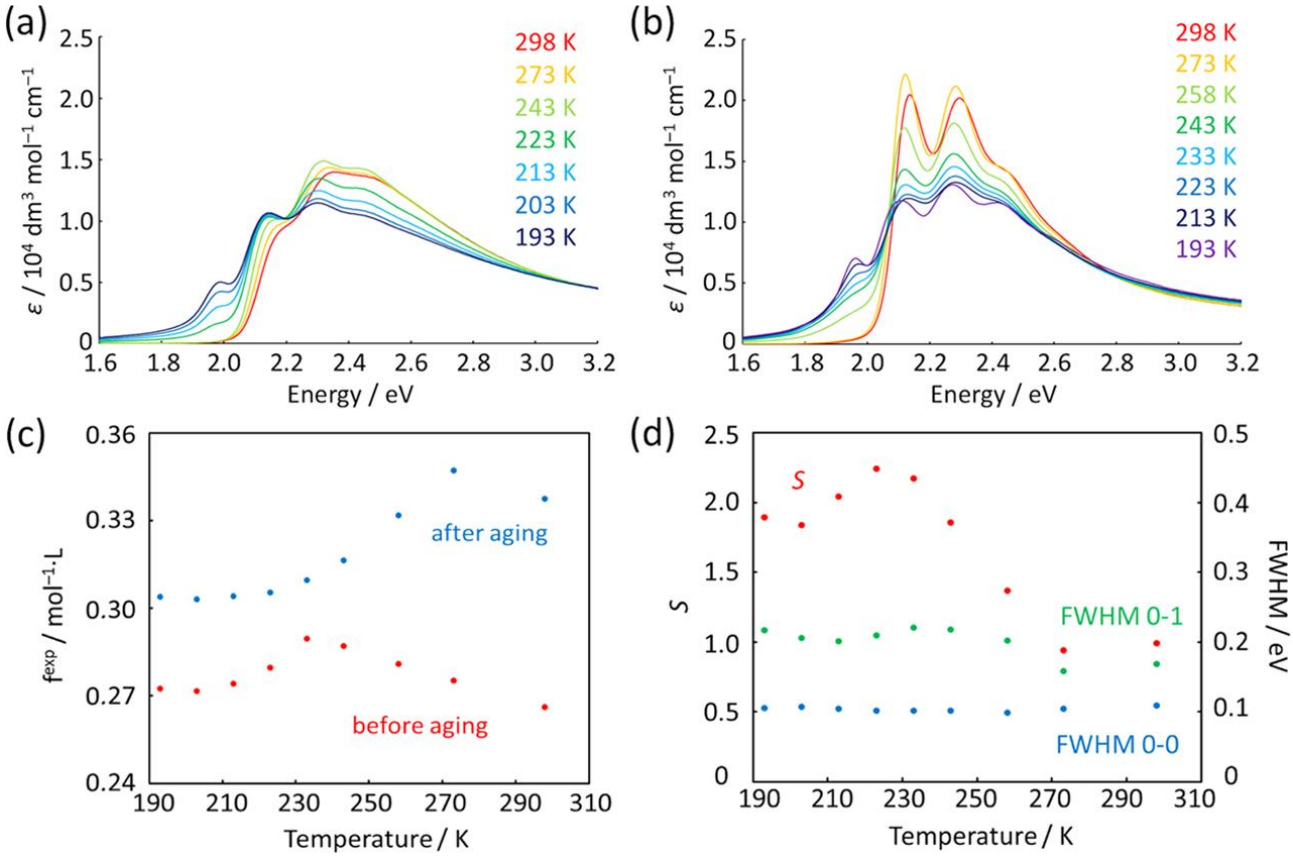

Figure 5. Extinction coefficient of **C6−C1F5** (c = 6.6×10^{-5} M) (a) before and (b) after aging in THF at various temperatures. (c) Oscillator strength of **C6−C1F5** before and after aging in THF at various temperatures. (d) The Huang−Rhys factor S (red) and full width at half-maximum (FWHM) of the 0−0 (blue) and the 0−1 (green) vibronic peaks of **C6−C1F5** in the Gaussian function at various temperatures.

resulting transition shifts toward lower; this is the case giving a new peak at around 1.9 eV via the J-type aggregates of conjugated segments. The *S* parameter jumped dramatically from 1.0 to 2.2. The jump was associated with the appearance of the new peak, where the aggregation of the rod–like chains occurred (Figure 5d). The aggregation of the conjugated chains facilitates the interchain conjugation that was well represented by the evident bathochromic shift in the new peak. It is evident that the new peak grows with the consumption of the 0→1 transition predominantly as seen in Figure 5a, while the intensity of the 0→0 transition is almost constant. This gives a decrease in S upon cooling and hence the extension of effective conjugation length due to aggregation of the conjugated backbone (Figure 5d). The value of FWHM of each vibrational peak for **C6−C2F4** and **C6−C1F5** was almost constant at the temperature where the aggregation occurred (Table 1). This is because the backbone was shielded and structurally confined by a 5- membered-ring and side chains, so that the vibrational mode of the conjugated chains was not suppressed even when the aggregate was formed.

The spectroscopic results so far revealed that the introduction of semifluoroalkyl chains accelerates the aggregation of the PA main chains and the length of fluorinated segments affects the thermal stability of the aggregates. A simple increase of concentration did not result in the aggregation behavior for the nonfluorinated **C6−C6** polymer (Figure 6).

The solvophobic and dipole−dipole interactions of fluoroalkyl segments are considered to be the dominant reasons for the aggregation.[52] An analogous polymer with higher fluorine content, **C2F4−C2F4** (Scheme 1), was synthesized and investigated by absorption spectroscopy. Similar to the cases of **C6−C2F4** and **C6−C1F5**, a shoulder peak at ~2.0 eV appeared upon decreasing the temperature of the THF solutions of **C2F4−C2F4** both before/after aging (Figure 7a,b). It should be noted that this peak was even observed at room temperature (~298 K) after the aging protocol, indicating the stronger thermal stability of the aggregates. Upon heating up to 333 K, the shoulder peak gradually disappeared and the vibronic absorption bands became more obvious (Figure 7c). This spectral change was reversible upon heating and cooling (Figure 7c,d).

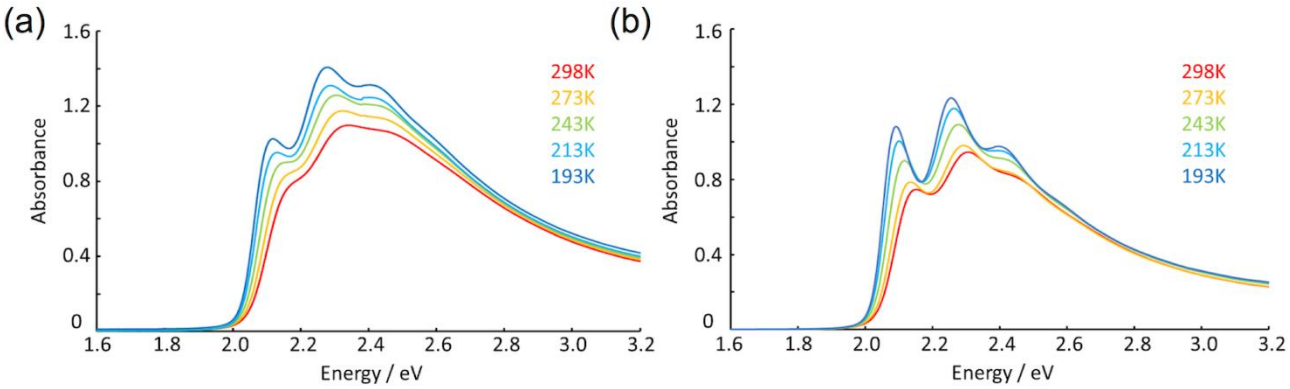

Figure 6. Electronic absorption spectra of **C6–C6** (a) before and (b) after aging in THF solution ($c = 1.0 \times 10^{-2}$ M) at various temperature. A quartz cell with an optical length of 0.05 mm was

Although absorption spectroscopy is powerful for studying the association of chromophore segments, it is difficult to discriminate intra and interchain aggregations explicitly. Dynamic light scattering (DLS) measurements were carried out to further support the interchain aggregation proposed in Scheme 2. The scattering profiles were recorded at room temperature (298 K) and a higher temperature (323 or 328 K). Figure 8 shows the representative distributions of the hydrodynamic diameter analyzed by the DLS measurements of diluted THF solutions of the polymers. The observation of scattering from the sizes of D_h = 1−10 nm is reasonable for the isolated single polymer chain with random coil conformations. In sharp contrast, much larger sizes

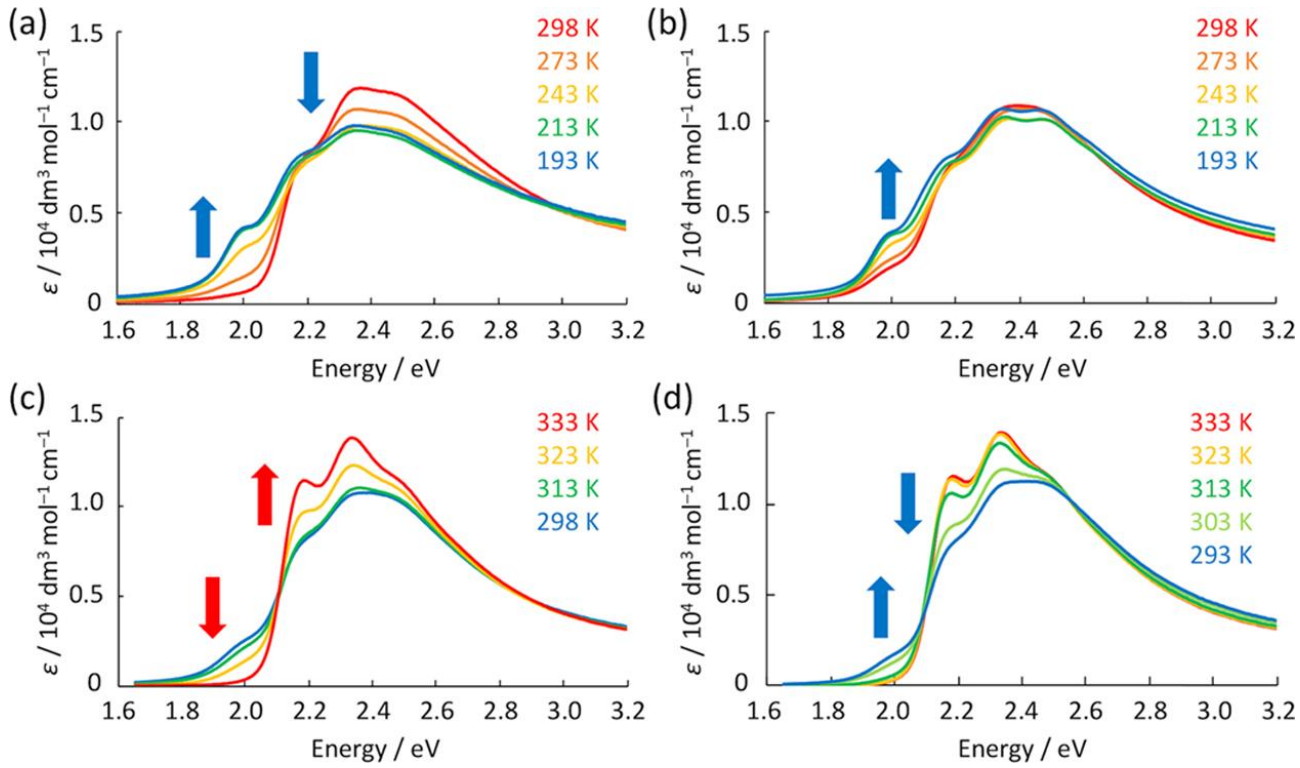

Figure 7. Extinction coefficient of **C2F4−C2F4** (c = 9.0×10^{-5} M) (a) before and (b) after aging in THF at various temperatures below room temperature. The extinction coefficient of **C2F4−C2F4** (c = 8.1×10^{-5} M) after aging in THF at various temperatures over room temperature on (a) heating and (b) cooling.

Scheme 2. Schematic Representation Depicting the Coil-to-Rod Transition for (a) C6−C6 and (b) C6−C2F4/C6−C1F5 via Photoisomerization and Further Self-Assembly To Stabilize the Rod Conformation upon Cooling

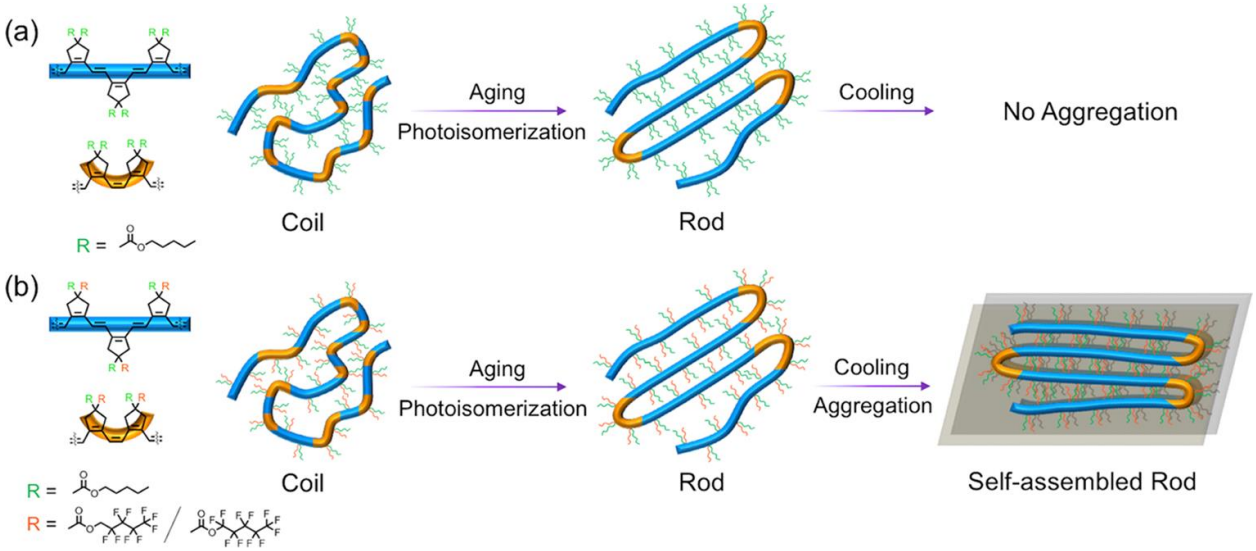

of D_h = ~500 and ~1000 nm were observed for **C2F4−C2F4** before and after aging respectively, which supports the interchain aggregation predicted by the absorption spectra in Figure 7. The sizes were decreased down to ~100 nm by increasing the temperature to 328 K for the polymers both before and after aging. The absorption and DLS results allow the conclusion that the absorption spectral changes by decreasing the temperature for **C6−C2F4**, **C6−C1F5**, and **C2F4−C2F4** solutions are the consequence of interchain aggregation of PA backbones induced by the side-chain fluoroalkyl segments.

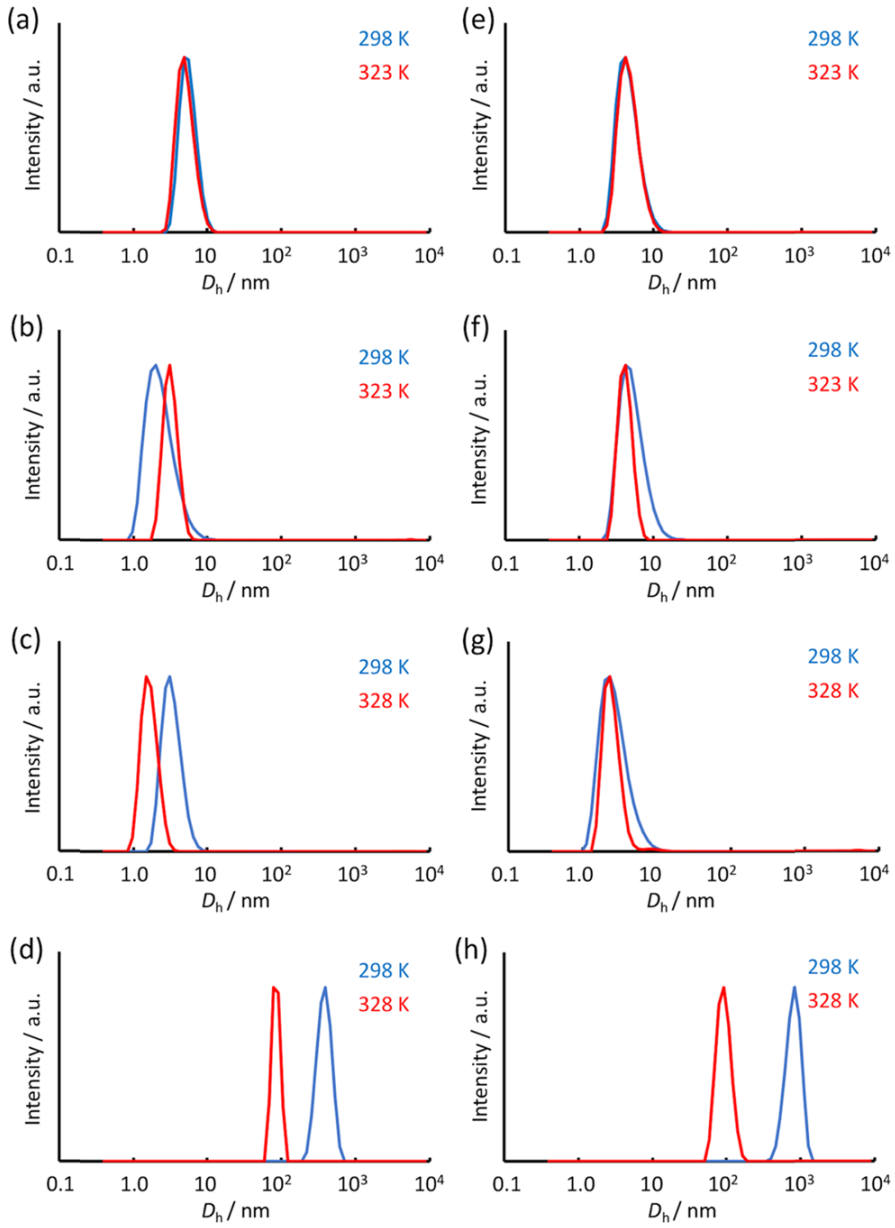

Figure 8. Hydrodynamic diameter distributions of (a) **C6−C6** before aging (c = 7.9×10^{-5} M), (b) **C6−C2F4** before aging (c = 8.3×10^{-5} M), (c) **C6−C1F5** before aging (c = 8.1×10^{-5} M), (d) **C2F4−C2F4** before aging (c = 9.4×10^{-5} M), (e) **C6−C6** after aging, (f) **C6−C2F4** after aging, (g) **C6−C1F5** after aging, and (h) **C2F4−C2F4** after aging, analyzed by dynamic light scattering in THF at 298, 323, or 328 K.

To confirm the aggregation of the polymers at low temperature, precise NMR spectroscopies were carried out by the difference NOE for **C6−C6** and **C6−C1F5** (Figures 9−11).

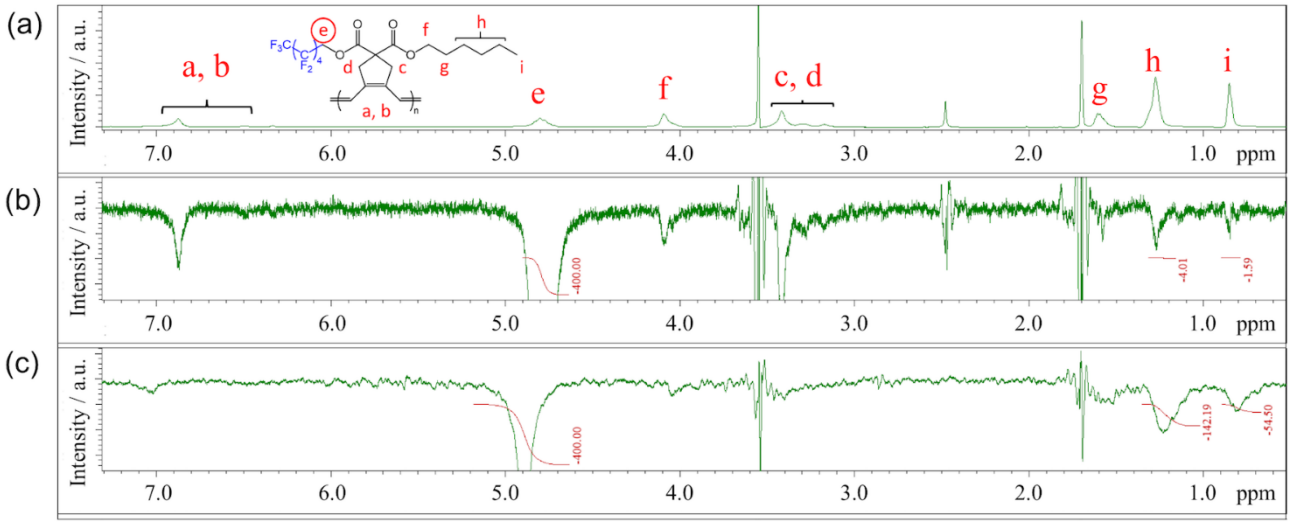

Figure 9. (a) ^{1}H NMR spectra of **C6–C1F5** in THF-d8 1D difference NOE with selective irradiation of proton e at (b) 293 K and (c) 223 K.

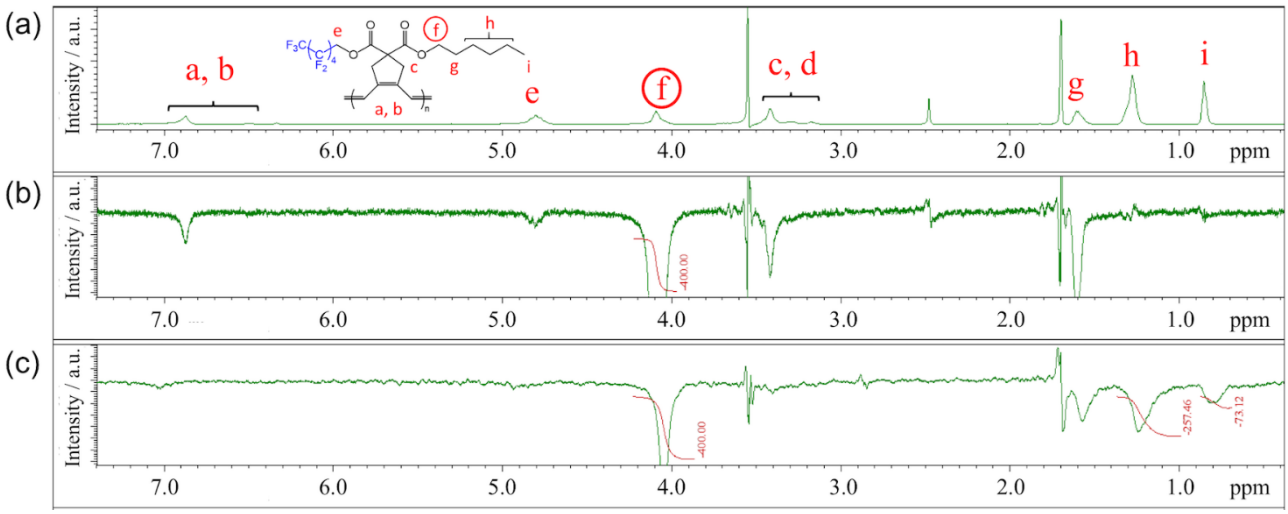

Figure 10. (a) ^{1}H NMR spectrum of **C6–C1F5** in THF-d8 at 293 K and 1D difference NOE with selective irradiation of proton f at (b) 293 K and (c) 223 K.

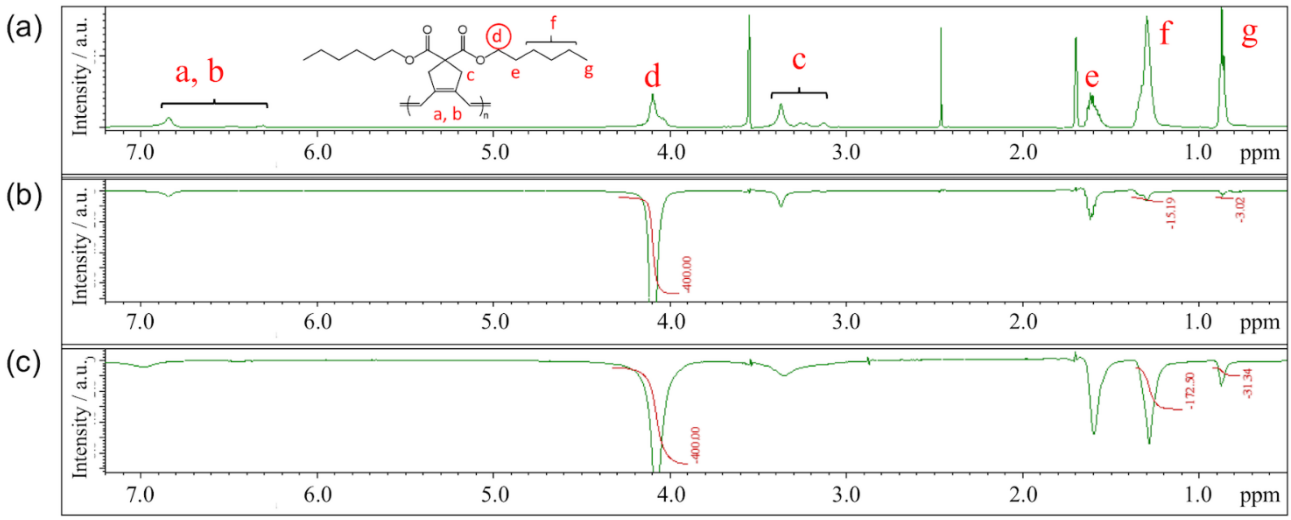

Figure 11. (a) ^{1}H NMR spectrum of **C6–C6** in THF-d8 at 293 K and 1D difference NOE with selective irradiation of proton d at (b) 293 K and (c) 223 K.

However, the long relaxation time of the protons gave negative NOE signals, which is due to the spin diffusion limit in the molecules with high molecular weight.[53−55] Double-pulsed field gradient spin-echo (DPFGSE) NOE spectra was examined and corrected. Two nonselective 180° pulses spaced within this interval can suppress the longitudinal magnetization arising during the mixing time due to relaxation. Thus, DPFGSE NOE is suitable for polymers with high molecular weights.[56,57] The interdistance of protons in the aggregated forms of the polymers was discussed below by DPFGSE NOE spectra.

Figure 12 shows the DPFGSE NOESY spectra for **C6−C1F5** with selective inversion of proton e in a 200 ms mixing time. Generally in NOE spectra, the correlation among protons whose interdistance one within 0.6 nm contributes remarkably in the spectra as the NOE signals. It is reasonable that no NOE peak was observed in 1.31 and 1.63 ppm at 293 K, which were assigned to the signals from protons g and h, respectively, where the polymer chain was isolated (Figure 12b). However, the intensity of both the signals showed an increase upon cooling down to 253 K (Figure 12c). This is suggestive that the spin correlation between e and g or h in the interchain

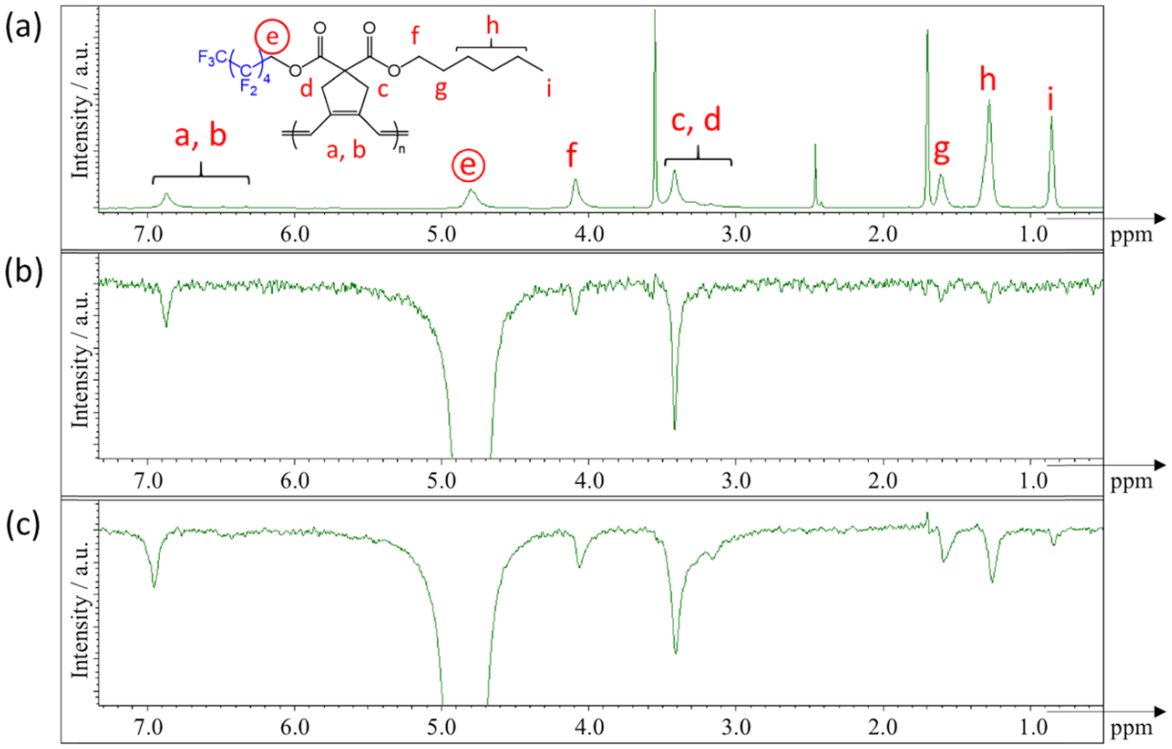

Figure 12. (a) 1H NMR spectra of **C6−C1F5** (c = 5.0×10^{-2} M) in THF-d8 at 293 K and DPFGSE NOE spectra with selective inversion of proton e at (b) 293 K and (c) 253 K. The mixing time was 200 ms.

manner (direct effect) was remarkable due to the formation of the aggregates upon cooling, but it is also possible that the intramolecular spin diffusion (indirect effect) affected the far away proton in the isolated chain because the backbone was stabilized upon cooling.[53–55] When proton e was irradiated selectively, it is assumed that only the direct effect would contribute to the NOE peak of proton d, which is spatially close to proton e, and both the direct and indirect effects would give the NOE peaks of protons g and h, which are spatially far away from proton e. The NOE intensity ratios of protons g/d and h/d were plotted against temperature and mixing time (Figures 13 and S10). Using a mixing time of 500 ms, both the intensity ratios increased monotonically with decreasing temperature, suggesting that intramolecular spin diffusion had an impact more significantly as the backbone was more stabilized upon cooling. Furthermore, the experiment was

repeated for mixing times of 50, 100, 200, and 500 ms at 253 K, resulting in the fact that the value of the intensity ratios was almost constant in the range from 50 to 200 ms, whereas the ratio at 500 ms was larger (Figure 14). These DPFGSE NOE results implied that the effect of intramolecular spin diffusion was negligible in the range from 50 to 200 ms; thus, the NOE signals were contributed dominantly by the direct effect derived from protons e and g or h belonging to the nearby but separate chains in the aggregates.

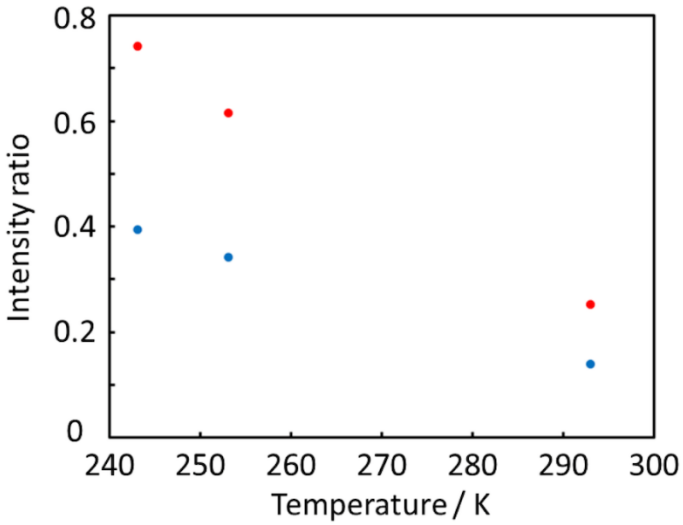

Figure 13. DPFGSE NOE intensity ratio of the proton g/d (red) and h/d (blue) for **C6–C1F5** in THF-d8 as a function of temperature. The proton e was inverted selectively and a mixing time of 500 ms was used.

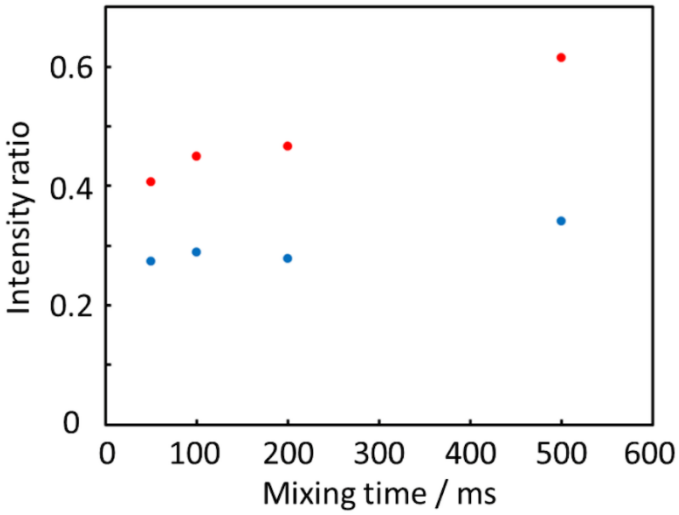

Figure 14. (a) DPFGSE NOE intensity ratio of the proton g/d (red) and h/d (blue) for **C6–C1F5** in THF-d8 at 253 K as a function of mixing time. The proton e was inverted selectively.

2.4 Conclusion

The aggregation dynamics of the substituted soluble polyacetylenes was examined by electronic absorption spectra at various temperature. Fluoroalkyl–Alkyl asymmetric substituted polymer (**C6-C2F4** and **C6-C1F5**) showed the formation of the aggregates with clear new peak at around 1.9 eV upon cooling, reducing the total transition dipoles by the cancellation of each transition dipoles. DPFGSE NOE also supported the formation of the aggregates at low temperature. When a long mixing time (500 ms) was used, intramolecular spin diffusion contributed in a large way to the NOE peaks. However, this effect was negligible in a shorter mixing time because the direct effect dominantly had an impact on the NOE signals. The simple introduction of semifluoroalkyl chains was found to serve as an efficient tool for controlling the aggregation behavior of soluble PA derivatives. The finding demonstrated in this work would give a general strategy to stabilize a particular conformer of polymer for practical applications.[58−60]

2.5 Reference

(1) G.Natta, G.Mazzanti, P.Corradini, *Cl. Sci. Fis.*, Mat. Nat., Rend. (1958), **25**, 3.

(2) H.Shirakawa, S.Ikeda, *Polym. J.*, (1971), **2**, 231−244.

(3) H.Shirakawa, E. J.Louis,; A. G.MacDiarmid, C. K.Chiang, A.J.Heeger, *J. Chem. Soc., Chem. Commun.* (1977), 578−580.

(4) W. P.Su, J. R.Schrieffer, A.J.Heeger, *Phys. Rev. Lett.*, (1979), **42,** 1698−1701.

(5) W. P.Su, J. R.Schrieffer, A.J.Heeger, *J. Phys. Rev. B*, (1980), **22**, 2099−2111.

(6) L. L.Böhm, *Polymer*, (1978), **19**, 562−566.

(7) A.Muñoz-Escalona, J. G.Hernandez, J. A.Gallardo, *J. Appl. Polym. Sci.*, (1984), **29**, 1187−1202.

(8) P.Pokasermsong, P.Praserthdam, *Eng. J.*, (2009), **13**, 57−64.

(9) P.Pletcher, A.Welle, A.Vantomme, B. M. Weckhuysen, *J.Catal.*, (2018), **363**, 128−135.

(10) E. H.Kang, I. S.Lee, T. L.Choi, *J. Am. Chem. Soc.*, (2011), **133**, 11904−11907.

(11) E.-H.Kang, I.-H.Lee, T.-L.Choi, *ACS Macro Lett.*, (2012), **1**, 1098−1102.

(12) E. H.Kang, T. L.Choi, *ACS Macro Lett.*, (2013), **2**, 780−784.

(13) E. H.Kang, S. Y.Yu, I. S.Lee, S. E.Park, T. L.Choi, *J. Am. Chem. Soc.*, (2014), **136**, 10508−10514.

(14) H.Jung, K.Jung, M.Hong, S.Kwon, K.Kim, S. H.Hong, T. L.Choi, M. H.Baik, *J. Am. Chem. Soc.*, (2018), **140**, 834−841.

(15) I.Choi, S.Yang, T. L. P. Choi, *J. Am. Chem. Soc.*, (2018), **140**, 17218−17225.

(16) G. I.Peterson, S.Yang, T.-L.Choi, *Acc. Chem. Res.*, (2019), **52**, 994−1005.

(17) U.Anders, O.Nuyken, M. R. Buchmeiser, *Des. Monomers Polym.*, (2003), **6**, 135−143.

(18) K.Akagi, *Chem. Rev.*, (2009), **109**, 5354−5401.

(19) M.Kyotani, S.Matsushita, T.Nagai, Y.Matsui, M.Shimomura, A.Kaito, K.Akagi, *J. Am. Chem. Soc.*, (2008), **130**, 10880−10881.

(20) M.Goh, M.Kyotani, K.Akagi, *J. Am. Chem. Soc.*, (2007), **129**, 8519−8527.

(21) M.Muthukumar, C. K.Ober, E. L.Thomas, *Science*, (1997), **277**, 1225−1232.

(22) P. M.Beaujuge, J. M.Frechet, *J. J. Am. Chem. Soc.*, (2011), **133**, 20009−20029.

(23) J. L.Koenig, D. E.Witeeiafer, *Macromol. Chem.*, (1966), **99**, 193−201.

(24) J. M.Huang, F. C.Chang, *J. Polym. Sci. Part B: Polym. Phys.*, (2000), **38**, 934−941.

(25) B.Wang, S.Watt, M.Hong, B.Domercq, R.Sun, B.Kippelen, D. M.Collard, *Macromolecules*, (2008), **41**, 5156−5165.

(26) K. B.Woody, R.Nambiar, G. L.Brizius, D. M.Collard, *Macromolecules*, (2009), **42**, 8102−8111.

(27) K.Tahara, C. A.Johnsn, T.Fujita, M.Sonoda, F. C. D.Schryver, S. D.Feyter, M. M.Haley, Y.Tobe, *Langmuir*, (2007), **23**, 10190−10197.

(28) T.Suwa, M.Takehisa, S.Machi, *J. Appl. Polym. Sci.*, (1973), 17, 3253−3257.

(29) J. C.Wittmann, P.Smith, *Nature*, (1991), **352**, 414−417.

(30) U.Dahn, C.Erdelen, H.Ringsdorf, R.Festag, J. H.Wendorff, P. A.Heiney, N. C.Maliszewskyj, *Liq. Cryst.*, (1995), **19**, 759.

(31) V.Percec, G.Johansson, G.Ungar, J.Zhou, *J. Am. Chem. Soc.*, (1996), **118**, 9855−9866.

(32) B. M.Rosen, C. J.Wilson, D. A.Wilson, M.Peterca, M. R.Imam, V.Percec, *Chem. Rev.*, (2009), **109**, 6275− 6540.

(33) C.Tschierske, *Angew. Chem. Int. Ed.*, (2013), 52, 8828−8878.

(34) Y.Tsutsui, T.Sakurai, K.Kato, M.Takata, S.Seki, *J. Photopolym. Sci. Technol.*, (2015), **28**, 583−587.

(35) T.Sakurai, Y.Tsutsui, K.Kato, M.Takata, S.Seki, *J. Mater. Chem. C*, (2016), **4**, 1490−1496.

(36) F.Panzer, H.Bassler, A.Kohler, *J. Phys. Chem. Lett.*, (2017), **8**, 114− 125.

(37) T.Mondal, T.Sakurai, S.Yoneda, S.Seki, S.Ghosh, *Macromolecules*, (2015), **48**, 879−888.

(38) A.Mukherjee, T.Sakurai, S.Seki, S.Ghosh, *ChemNanoMat*, (2018), **4**, 860−866.

(39) K.Huang, A.Rhys, *Proc. R. Soc. London, Ser. A*, (1950), **204**, 406−423.

(40) K.Pichler, D. A.Halliday, D. D. C.Bradley, P. L.Burn, R. H.Friend, A. B.Holmes, *J. Phys.: Condens. Matter*, (1993), **5**, 7155− 7072.

(41) Z.Shuai, J. L.Bredas, W.P.Su, *Chem. Phys. Lett.*, (1994), **228**, 301−306.

(42) J.Cornil, D.Beljonne, Z.Shuai, T. W.Hagler, I.Campbell, D. D. C.Bradley, J. L.Bredas, C. W.Spangler, K.Müllen, *Chem. Phys. Lett.*, (1995), **247**, 425−432.

(43) J. W.Blatchford, S. W.Jessen, L. B.Lin, T. L.Gustafson, D. K.Fu, H. L.Wang, T. M.Swager, A. G.MacDiarmid, A.Epstein, *J. Phys. Rev. B*, (1996), **54**, 9180−9189.

(44) J.Yu, M.Hayashi, S. H.Lin, K. K.Liang, J. H.Hsu, W. S.Fann, C. I.Chao, K. R.Chuang, Chen, S. A. Synth. Met., (1996), **82**, 159−166.

(45) S.Quan, F.Teng, Z.Xu, L.Qian, T.Zhang, D.Liu, Y.Hou, Y.Wang, X.Xu, *J. Lumin.*, (2007), **124**, 81−84.

(46) J.Kordas, P.Avourls, M. A. E.Bayoumi, *J. Phys. Chem.*, (1975), **79**, 2420−2423.

(47) S.Seki, Y.Koizumi, K.Nishida, Y.Yoshida, S.Tagawa, *J. Phys. Chem. B*, (2001), **105**, 900−904.

(48) S.Seki, Y.Matsui, Y.Yoshida, S.Tagawa, *J. Phys. Chem. B*, (2002), **106**, 6849−6852.

(49) S.Seki, Y.Koizumi, T.Kawaguchi, H.Habara, S.Tagawa, *J. Am. Chem. Soc.*, (2004), **126**, 3521−3528.

(50) M.Kasha, H. R.Rawls, M. A.E-bayoumi, *Pure Appl. Chem.*, (1965), **11**, 371−392.

(51) S.Ghosh, D. S.Philips, A.Saeki, A.Ajayaghosh, *Adv. Mater.*, (2017), **29**, No. 1605408.

(52) T.Hasegawa, Chem. Rec., (2017), **17**, 903−917.

(53) J.Forbes, J.Bowers, X.Shan, L.Moran, E.Oldfield, M. A.Moscarello, *J. Chem. Soc.*, (1988), **84**, 3821−3849.

(54) Z. J.Chen, R. E.Stark, *Solid State Nucl. Magn. Reson.*, (1996), **7**, 239−246.

(55) D.Huster, K.Arnold, K.Gawrisch, *J. Phys. Chem. B*, (1999), **103**, 243−251.

(56) K.Stott, J.Keeler, Q. N.Van, A. J.Shaka, *J. Magn. Reson.*, (1997), **125**, 302−324.

(57) H.Hu, K.Krishnamurthy, *J. Magn. Reson.*, (2006), **182**, 173−177.

(58) D. T.McQuade, A. E.Pullen, T. M.Swager, *Chem. Rev.*, (2000), **100**, 2537−2574.

(59) S. W.Thomas, G. D.Joly, T. M.Swager, *Chem. Rev.*, (2007), **107**, 1339−1386.

(60) T. M.Swager, *Macromolecules*, (2017), **50**, 4867−4886.

Chapter 3

Impacts of Thermal Fluctuation on Opto-Electronic Properties of Microcrystalline Oligophenyleneethynylene Chains: An Analog of Crystalline Domains of Linear Conjugated Polymers

3.1 Introduction

The optical properties of conjugated polymers are impacted not only by the primary chemical structure, but also by the configuration of the polymer chains and the inter-chain interactions. Conjugated polymers have often been anticipated to be applied in their amorphous form in thin solid films, considering such advantages as flexibility and printability; however, this conflicts with the desirable characteristics of their regularly aligned forms/crystallites with respect to their optoelectronic properties in condensed phases [1]. It has been reported that such regularly aligned forms have a significant impact on the charge transport properties[2]. However, crystalline phases of polymeric materials do coexist with their amorphous counterparts, and perfect single crystals have long been pursued in the field of solid state polymeric materials. Tie chains that connect crystallites of polymers have been revealed to play an important role in charge carrier transport[3,4]. Charge transport in direct-current (DC) mode reflects overpassing processes in these tie chains,

which results in breakdown by the chains over the entire process. This has also been suggestive of the importance of crystalline domains to facilitate efficient/smooth charge transport pathways in highly developed crystalline domains of conjugated polymer chains. The flash photolysis-time-resolved microwave conductivity (FP-TRMC) measurement technique is a contactless evaluation method of intra-crystalline domain motion and the charge carriers in alternating-current (AC) modes[5]. In FP-TRMC, transient charge carriers are injected into the domains via photoionization, and the coexisting disordered parts of the polymers are often expected to immobilize counter charges via localization of the charges by strong electron-phonon coupling and/or trapping with impurities[6,7]. The features in solid phase diagrams of macromolecular chains are generally dependent on the average chain length and distribution[8]. Oligomer analogs of identical conjugated chromophores with shorter chains and no distribution are expected to enrich the crystallinity, and thus simulate the inherent electrooptical properties of the conjugated backbones[9].

Poly/oligo-*p*-phenylene ethynylenes (PPE/OPE) are simple and linear conjugated macromolecular systems with relatively long persistence length in the backbone configurations[10]; they are an ideal motif to address the impact of oligomer aggregation on their properties. OPEs with long alkyl peripheries have been systematically synthesized up to heptamers and their condensed phases have been characterized[11]. Supramolecular aggregated structures of OPEs with shorter alkyl peripheries exhibit characteristic phase behavior in contrast to simple solid-isotropic transition (T_m) of OPEs; however, no detailed discussion has been given with regard to the microscopic structural changes in the transition below T_m. I have also reported on the optoelectronic properties of poly(2,5-dioctyloxy-*p*-phenylene)ethynylene that yields ordered aggregates with suppression of the twisting and rotational motion of the intrachain units, even in solution at low temperatures in chapter 1[12]. The morphology and associated optical properties in condensed phases/films of phenylene

ethynylene oligomers have often been subjects of debate[13,14]; the electronic properties including the charge carrier mobility are still unclear at this stage. Here, I synthesize oligo(2,5-butoxy-*p*-phenylene ethynylene) with distinct chain lengths: trimer (**P3**) and pentamer (**P5**). The impact of thermal fluctuation on the optoelectronic properties of microcrystalline oligo(phenylene ethynylene) were investigated both in solution and in the solid film state.

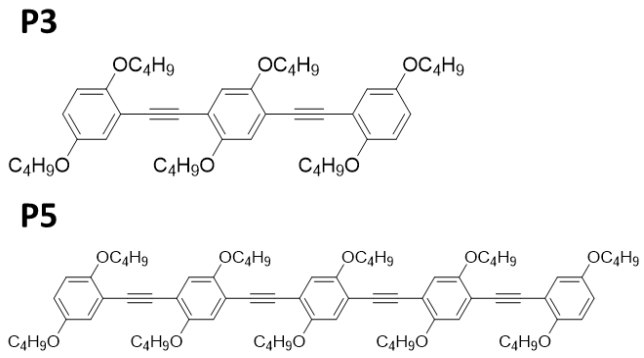

Figure 1. The chemical Structure of **P3** and **P5**.

3.2 Experimental Section

Unless otherwise noted, all commercial reagents were purchased from Wako Pure Chemical Industries Ltd., Tokyo Chemical Industry Co. Ltd., or Sigma-Aldrich Co., and used as-received. **P3** and **P5** were prepared by Sonogashira coupling reactions. The compounds were purified by recrystallization from solution in methanol.

Electronic absorption and fluorescence spectra of **P3** and **P5** were recorded in tetrahydrofuran (THF) as a solvent with an optical path length of 1 cm, or in pristine solid films coated onto quartz substrates. Differential scanning calorimetry (DSC) measurements were performed on a PerkinElmer DSC8000 calorimeter. X-ray diffraction (XRD) measurements of the mixtures were conducted using a Rigaku MiniFlex600 diffractometer (λ = 1.54Å) with a D/teX Ultra semiconductor detector. MALDI-TOF mass spectral data were obtained using a Bruker made flex series TOF/TOF instrument with laser repetition rate of 50 psec. 1,8,9-Anthracenetriol was used as the matrix for MALDI-TOF mass spectrometry. Electrochemical measurements of **P3** and **P5** were performed with cyclic voltammetry (CV) and differential pulse voltammetry (DPV) with a potentiostat (ALS 760E) in CH_2Cl_2 solutions using 0.1 M tetrabutylammonium tetrafluoroborate (*n*-Bu_4-NBF_4) as supporting electrolyte, Ag/AgCl as reference electrode, and platinum as working and counter electrode. FP-TRMC measurements were performed in a N_2 flow with a resonant cavity under various temperatures from 293 to 373 K. The third harmonic generation (THG; 355 nm) of a Nd:YAG laser (Spectra-Physics Inc., INDI, 5–8 ns pulse duration, 10 Hz) and X-band microwaves (*ca.* 9 GHz, 3 mW) were used as the excitation source and microwave probe, respectively. The photon density of the excitation pulse was set at 9.1×10^{15} photons per cm^2 per pulse. The film samples were prepared by drop-casting from chloroform solution (*ca*. 10 wt%)

onto quartz substrates, drying for 30 min. at room temperature, and then thermal annealing at the melting point of the corresponding compounds.

Synthetic Details

Scheme 1. Synthetic scheme of **P3** and **P5**

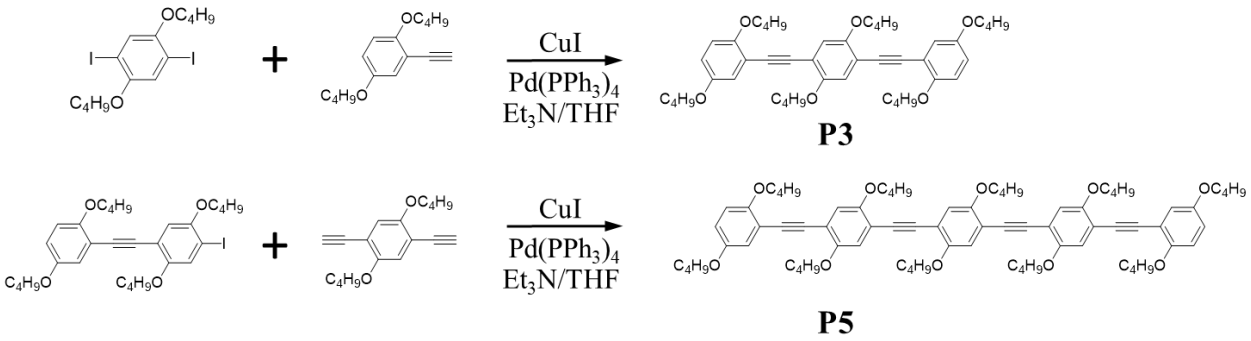

P3

To a dry Et_3N/THF solution (20 mL, 1/1 v/v) of 1,4-diiode-2,5-butoxybenzene (3.15 g, 6.64 mmol) and 1,4-diiode-2-ethynylbenzene (1.64 g, 6.64 mmol) were added $Pd(PPh_3)_4$ (383 mg, 0.33 mmol), and CuI (126 mg, 0.66 mmol), and the mixture was degassed by freeze-pump-thaw cycles for 3times. The mixture was evaporated to dryness under reduced pressure, dissolved in $CHCl_3$, and passed through a plug of SiO_2. After stirring at 60°C for 24 h, the mixture was evaporated to dryness under reduced pressure, dissolved in $CHCl_3$, and passed through a plug of SiO_2. Further purification and fractionation were carried out by a recycling preparative SEC using $CHCl_3$ as an eluent. The compounds were purified by recrystallization from methanol solution. Yield: 1.65 g (35%). ^{1}H NMR (400 MHz, $CDCl_3$) δ_H = 7.00 (m, 8H), 6.83 (2, 4H), 4.05 (m, 16H), 3.93 (t, 4H), 1.84 (m, 20H), 1.53 (m, 20H), 0.97 (m, 30H). ^{13}C NMR (400 MHz, $CDCl_3$) δ_C =13.8, 19.3, 31.4, 68.4, 69.4, 69.7, 90.0, 114.4, 116.7, 117.4, 118.5, 152.9, 153.5, 154.0.

P5

To a dry Et_3N/THF solution (3.0 mL, 1/1 v/v) of 1,4-butoxy-2,5diethynyl-benzene (170 mg, 0.63 mmol) and 1-iode-2,5-di(dodecanoxy)-4-((2,5-di(dodecanoxy)phenyl)ethynyl)benzene (932 mg, 1.57mmol) were added $Pd(PPh_3)_4$ (383 mg, 0.33 mmol), and CuI (126 mg, 0.66 mmol), and the mixture was degassed by freeze-pump-thaw cycles for 3times. The mixture was evaporated to dryness under reduced pressure, dissolved in $CHCl_3$, and passed through a plug of SiO_2. After stirring at 60°C for 24 h, the mixture was evaporated to dryness under reduced pressure, dissolved in $CHCl_3$, and passed through a plug of SiO_2. Further purification and fractionation were carried out by a recycling preparative SEC using $CHCl_3$ as an eluent. The compounds were purified by recrystallization from methanol solution. Yield: 452 mg (59%)

^1H NMR (400 MHz, $CDCl_3$) δ_H = 7.01 (m, 8H), 6.83 (2, 4H), 4.03 (m, 16H), 3.93 (t, 4H), 1.81 (m, 20H), 1.53 (m, 20H), 1.00 (m, 30H). ^{13}C NMR (400 MHz, $CDCl_3$) δ_C =13.9, 19.3, 31.4, 68.4, 69.3, 69.6, 89.8, 91.4, 91.6, 114.0, 114.1, 114.3, 114.6, 116.7, 117.4, 118.5, 152.9, 153.5, 154.0.

2.2.

3.2 Results and Disscussion

The chemical structures of **P3** and **P5** are illustrated in Figure 1. The compounds were unambiguously identified using ^{1}H and ^{13}C nuclear magnetic resonance spectroscopy (NMR) and matrix-assisted laser desorption ionization-time of flight mass spectrometry (MALDI-TOF-MS)

Figure 2 shows electronic absorption and fluorescence spectra, which indicate a significant bathochromic shift in **P5** relative to that of **P3**. This suggests the elongation of intramolecular conjugation proportional to the number of backbone units; the rod-like configuration of the chains is still preserved in both **P3** and **P5** that bear shorter total chain length than the persistence length of PPE.

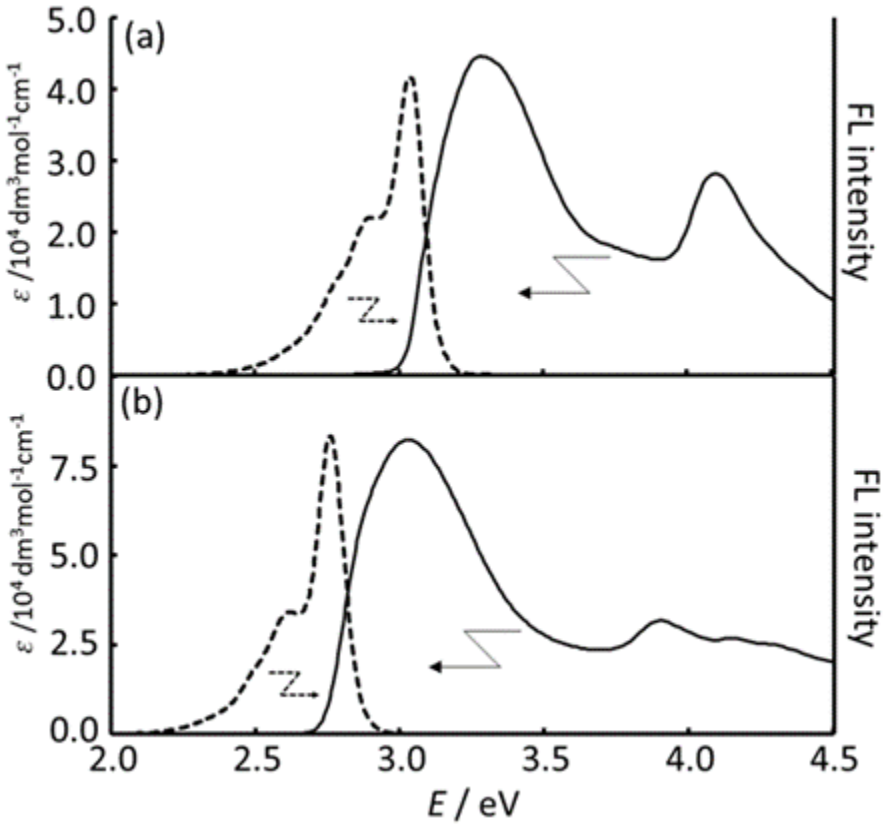

Figure 2. Electronic absorption spectra (solid lines) and fluorescence spectra (dotted lines) for (a) **P3** in THF ($c = 1.5\times10^{-5}$ M) and (b) **P5** in THF ($c = 1.0\times10^{-5}$ M).

Figure 3 shows DSC thermograms of **P3** and **P5**. A clear melting peak was observed at 366 K in **P3** (ΔH_m = 71.7 kJ mol^{-1}), which is associated with the crystallization peak at 336 K (ΔH_c = −46.3 kJ mol^{-1}) in the reverse scan. In contrast, **P5** shows an additional endothermic peak at 356 K (S1−S2, ΔH = 10.4 kJ mol^{-1}) other than a melting peak at 427 K (ΔH_m = 60.0 kJ mol^{-1}). It should be noted that the corresponding exothermic peaks were recorded in the reverse scan at 344 K (ΔH = 9.9 kJ mol^{-1}) and the crystallization peak at 403 K (ΔHc = −65.1 kJ mol^{-1}).

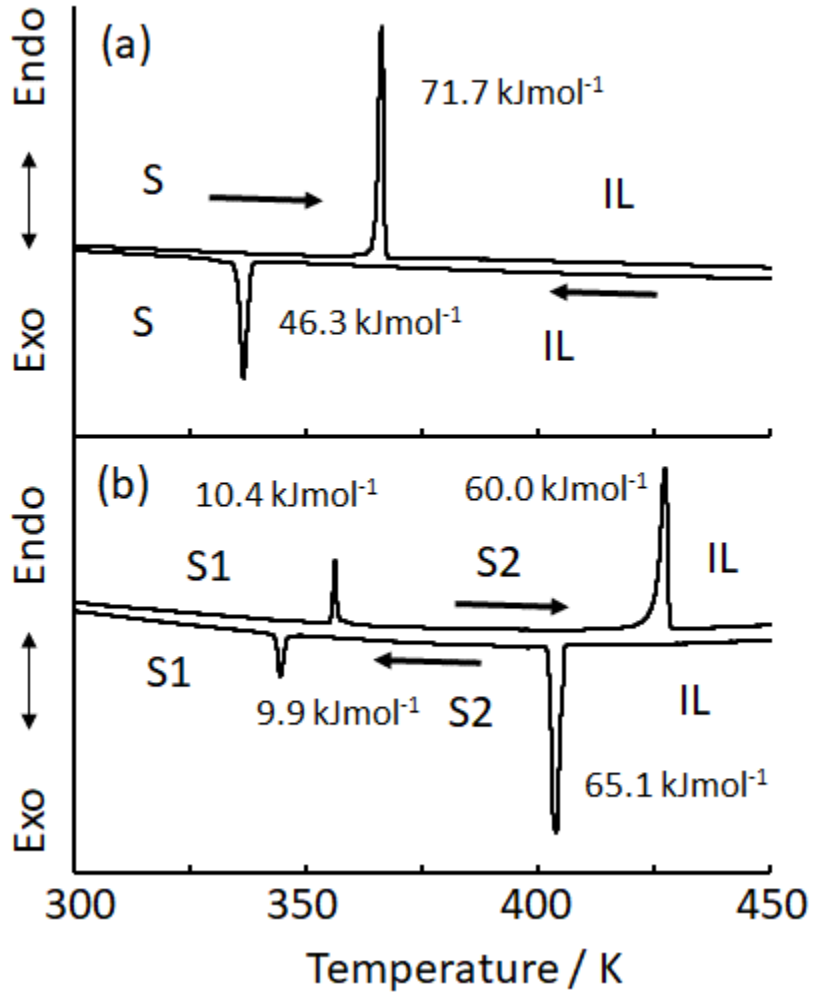

Figure 3. DSC curves of air-dried $CHCl_3$-cast films of (a) **P3** and (b) **P5** at 10 K min^{-1}

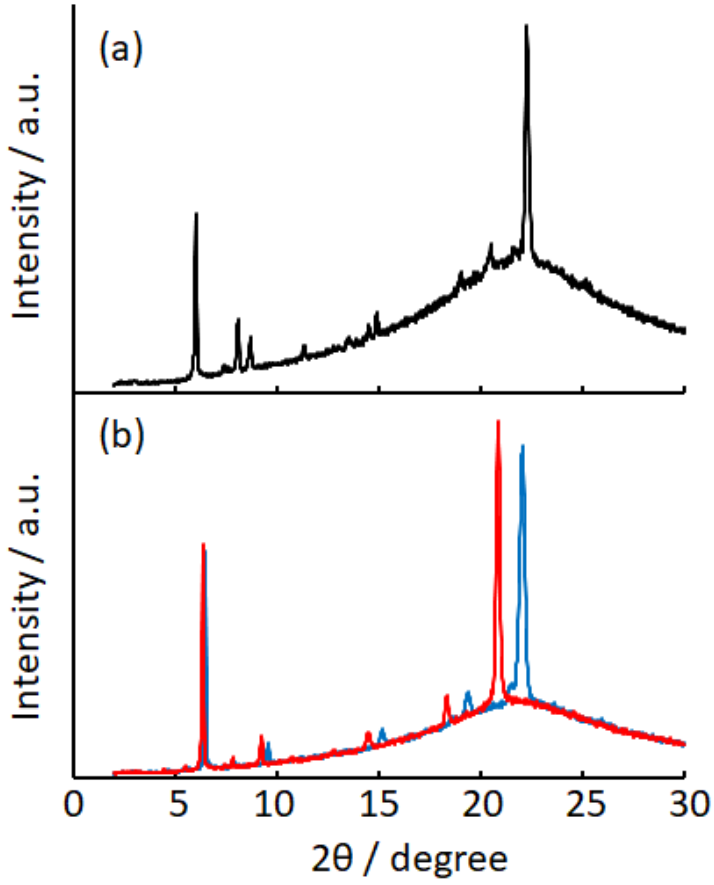

Figure 4. XRD patterns of (a) **P3** at 298 K and (b) **P5** at 298 K (blue) and 373 K (red).

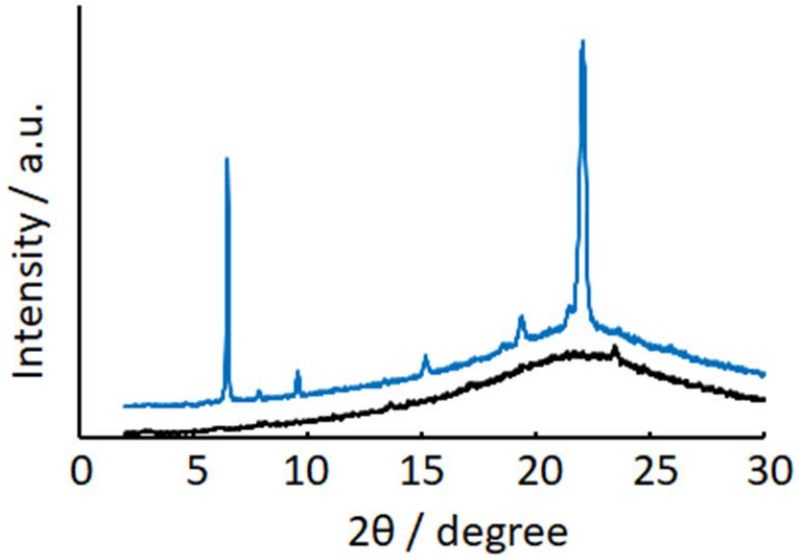

Figure 5. XRD pattern of **P5** at 298 K $CHCl_3$-dropcast film (black) and second cycles (blue).

Reproducibility/reversibility was confirmed for the S1−S2 endo/exothermic peaks around 344−356 K in successive thermograms, as represented in the second runs in Figure 4. The enthalpy change (ΔH) of the S1−S2 peak was recorded as one-sixth of ΔH_c: the transition into the isotropic liquid.

Temperature dependent XRD analyses were conducted for $CHCl_3$-cast films of **P3** and **P5** to confirm the condensed phase structures of **P3** and **P5**, and the results are also shown in Figure 5. All the patterns were recorded in the second heating cycles, and distinct double peaks were observed for **P5**. It was noteworthy that the diffraction pattern of the as-cast film of **P5** in the first heating cycle was almost featureless, which is in striking contrast to that for the melt-crystallized film after the second heating cycle; **P5** can be effectively crystallized during the first and later cooling processes. Almost identical patterns were obtained for both **P3** and **P5** at room temperature, which consisted of two major peaks with *d*-spacings of 1.45 and 0.399 nm in **P3**, and 1.36 and 0.403 nm in **P5**. The larger *d*-spacings at 1.36−1.45 nm represent the inter-molecular distances orthogonal to the rod-like molecular axes with interference by the long alkyl peripheries. Given that the chain lengths of the peripheries in **P3** and **P5** were identical, the slightly shorter *d*-spacing in **P5** may be due to interdigitation of the alkyl chains in the peripheries. The diffraction peaks at 0.399−0.403 nm were assigned to π-stacking of the conjugated backbones, which were ca. 6% extended from the reported π-stacking distances in PPEs[15,16]. No clear change was observed in the XRD pattern of **P3** upon heating, and the pattern became featureless above the melting point. In contrast, **P5** showed clear fingerprints of crystalline phases below and above the S1−S2 phase transition temperature, which was associated with a slight peak shift observed only for the π-stack spacing. Rod-like molecules with relatively higher molecular aspect ratios have often exhibited solid−mesophase transition, which leads to the nematic/smectic liquid crystalline phases[17,18].

However, the characteristic S1−S2 phase transition in **P5** is unlikely to be such a case, but rather a solid−solid transition, according to the XRD analyses. The stepwise change in the *d*-spacing of the π-stacking is due to partial melting of the peripheral alkyl chain ends, which plays a key role in the intermolecular locking via alkyl interdigitation[19].

Electronic absorption spectra of **P3** and **P5** films were measured in terms of intermolecular electronic coupling upon the S1−S2 phase transition (Figure 6). Despite the larger π-stacking distances, and thus the presumption of less electronic coupling, vibronic features appeared clearly.

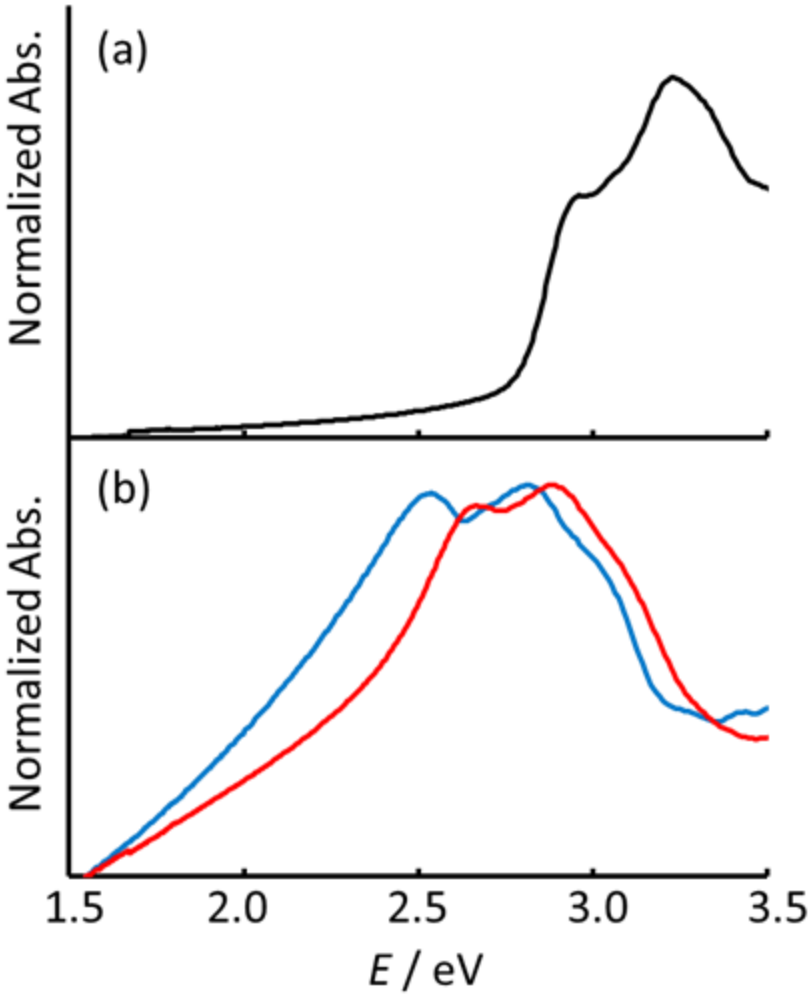

Figure 6. Electronic absorption spectra of $CHCl_3$-cast films of (a) **P3** at 298 K and (b) **P5** at 298 K (blue) and 373 K (red)

The relative transition dipole strength that represents vibronic modes provides key information on the spatial arrangements of adjacent conjugated backbones[20]. The dipole strength of the lowest energy 0−0 and the second 0−1 transitions have been a good indicator of the stacking mode. The results suggest J-type aggregates of **P5**, as evidenced by the larger transition dipole of the 0−0 transition.

No clear change was observed in the electronic absorption spectra of **P3** upon heating. In contrast, a significant blue shift of the absorption maxima was observed in **P5** upon heating from the S1 to S2 states, which can be attributed to a reduction in the intermolecular electronic coupling. The J-type stacking mode was still realized, even in the S2 phase of **P5** without change of the relative vibronic dipoles.

Here we discuss the simple solid-solid phase transition of **P5** with uniaxial anisotropic expansion and how it impacts the electronic transport in both phases. Intracrystalline domain local charge carrier motion was assessed by FP-TRMC measurement to address this question. CV as well as DPV spectra of **P3** and **P5** (Figure 7) show the first oxidation potential at 1.22 and 1.18 V (vs. ferrocene/ferrocenium) with small dependence on the chain length, suggesting equivalent photo

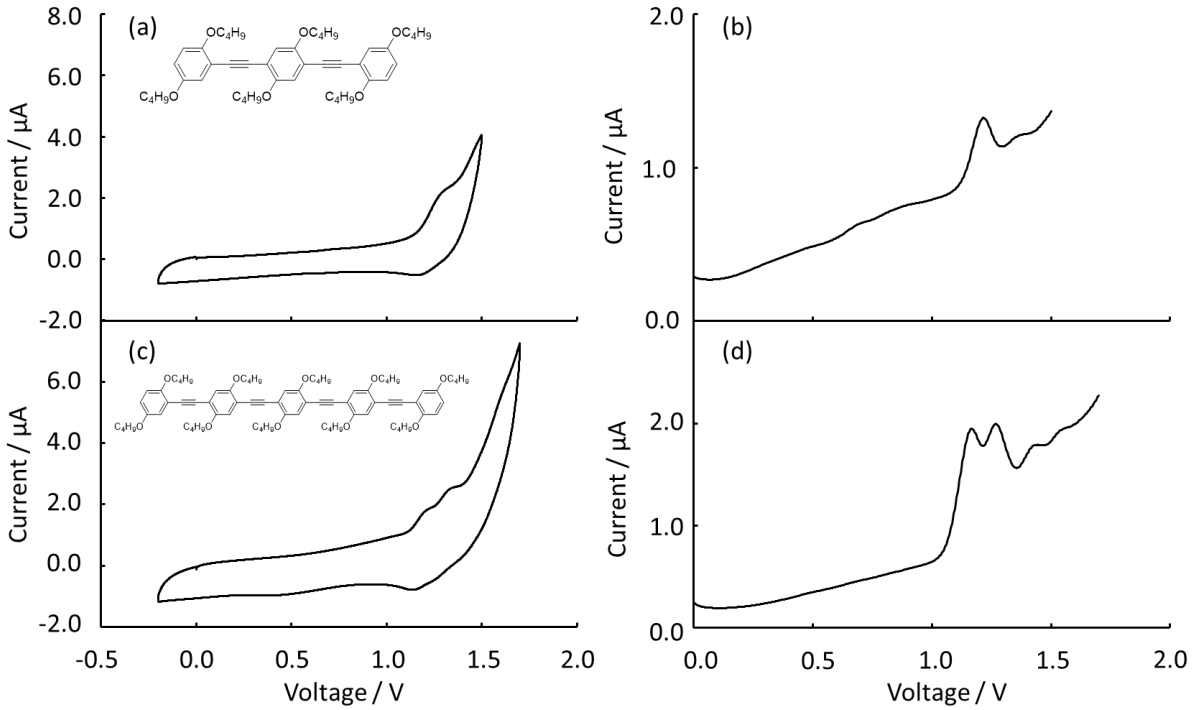

Figure 7. Cyclic Voltammetry (CV) and Differential Pulse Voltammetry (DPV) spectra of **P3** (a, b) and **P5** (c, d) in CH_2Cl_2 solutions using 0.1 M tetrabutylammonium tetrafluoroborate (*n*-Bu_4-NBF_4) as supporting electrolyte, Ag/AgCl as reference electrode, and platinum as working and counter electrode.

ionization yield upon excitation at 355 nm in FP-TRMC measurements.[21,22] **P3** exhibited a marked pseudo transient conductivity of 5.7×10^{-9} m^2 V^{-1} s^{-1} at 293 K, which was increased slightly up to 6.6×10^{-9} m^2 V^{-1} s^{-1} at 353 K. The weak intermolecular electronic coupling was expected both in **P3** and **P5**, as presumed by XRD and UV-vis measurements, and thus a thermally activated hopping regime is responsible in all the crystalline phases of these compounds. This is the case give small rise in the pseudo transient conductivity. On the other hand, the pseudo transient conductivity of **P5** was decreased slightly from 8.4×10^{-9} m^2 V^{-1} s^{-1} at 293 K to 7.9×10^{-9} m^2 V^{-1} s^{-1} at 373 K. Note that the conductivity was significantly higher in **P5** than in **P3**, but with negative temperature dependence. The uniaxial anisotropic expansion in **P5** causes a steep rise in the

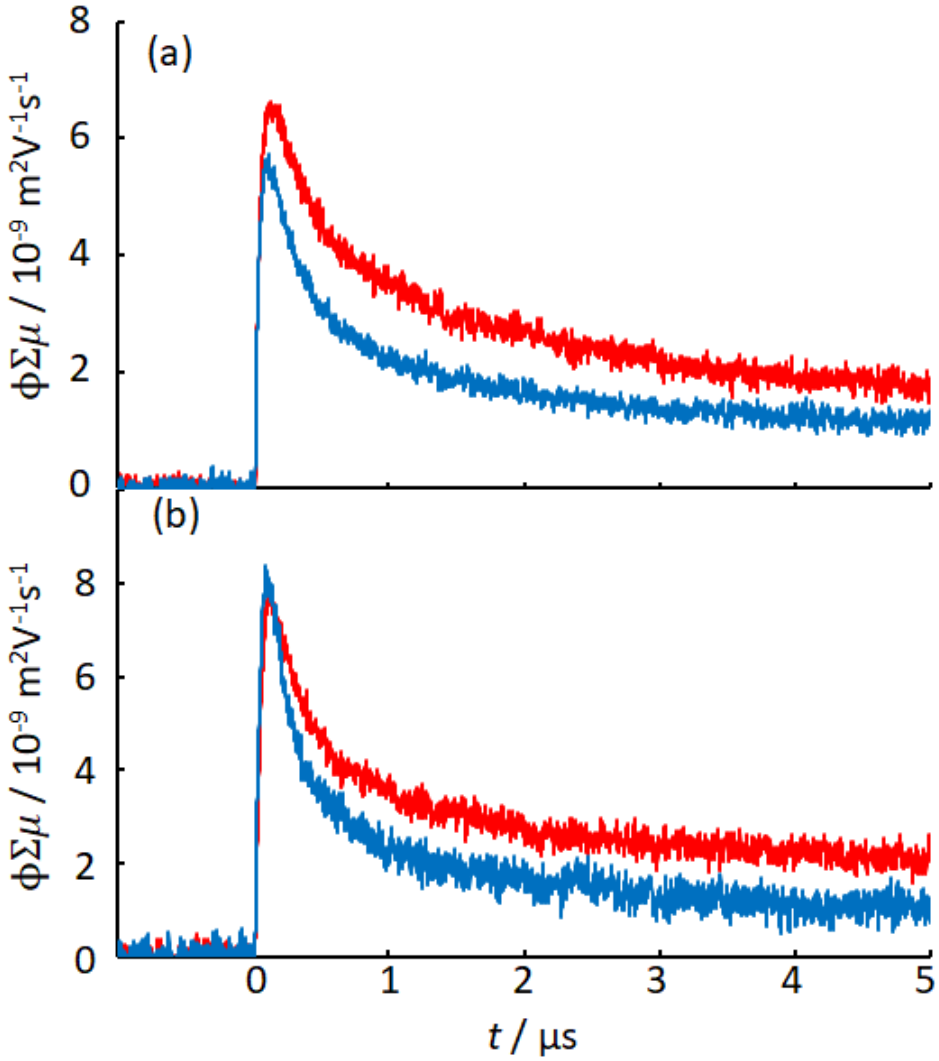

Figure 8. FP-TRMC photoconductivity transients recorded for (a) **P3** at 293 K (blue) and 353 K (red), and for (b) **P5** at 293 K (blue) and 373 K (red) upon excitation at 355 nm, 9.1×10^{15} photons per cm^2 per pulse. The samples were prepared by drop-casting from chloroform solution.

intermolecular hopping barrier, which leads to this contrasting result. A maximum of ca. 6% compression/expansion of crystalline unit cells is observed by pressurization/relaxation of typical van der Waals solids with similar long alkyl chain peripheries to as much as 0.5−1 GPa[23]. The conductivity change in the S1 and S2 phases of **P5** is consistent with that observed in the

pressurization/relaxation of poly(3-hexylthiophene) (P3HT) at room temperature. Another characteristic feature in the conductivity transients was in the decay kinetics, which exhibited long-lasting components, particularly in **P5** upon heating. Intermolecular gap expansion upon heating may suppress the bulk (Langevin) recombination of photogenerated electron–hole pairs.

3.4 Conclusion

The optoelectronic properties of the OPE trimer (**P3**) and pentamer (**P5**) were investigated as a function of temperature. A unique solid-solid phase transition was observed only in the analog of **P5** at 356 K. The phase transition can be assigned as uniaxial anisotropic expansion of the crystalline phase via the partial melting of interdigitated alkyl chain peripheries. The impact of the solid-solid phase transition was assessed with respect to the electronic conductivity in crystalline domains, which revealed that the thermal activation of charge carrier hopping interplayed with the reduction of intermolecular electronic coupling induced by uniaxial thermal expansion of the intermolecular π-stacking distance up to ca. 6%.

3.5 Reference

(1) A. Kolinski, J. Skolnick, R. Yaris, *J. Chem. Phys.*, (1986), **85**, 3585-3597.

(2) T. Yamamoto, K. Sanechika, *J. Polym. Sci., Polym. Lett.*, (1980), **18**, 9-12.

(3) A. Salleo, *Mater. Today,* (2007), **10**, 38-45.

(4) K. Gu, C. R. Snyder, J. Onorato, C. K. Luscombe, A. W. Bosse, Y. Loo, *ACS Macro Lett.*, (2018), **7**, 1333-1338.

(5) A. Saeki, S. Seki, Y. Koizumi, T. Sunagawa, K. Ushida, S. Tagawa, *J. Phys. Chem. B*, (2005),

109, 10015-10019.

(6) A. Saeki, S. Seki, T. Sunagawa, K. Ushida, S. Tagawa, *Philos. Mag.*, (2006), **86**, 1261-1276.

(7) S. Seki, S. Tagawa, *Polym. J.*, (2007), **39**, 277-293.

(8) Pierre-Gilles de Gennes, *Scaling Concepts in Polymer Physics*, Cornell University Press, Ithaca and London, 1979.

(9) R. J. Kline, M. D. McGehee, E. N. Kadnikova, J. Liu, J. M. J. Fréchet, M. F. Toney, *Macromolecules*, (2005), **38**, 3312-3319.

(10) J. H. Moon, T. M. Swager, *Macromolecules*, (2002), **35**, 6086-6089.

(11) G. Castruita, E. Arias, I. Moggio, F. Pérez, D. Medellín, Román Torres,R. Ziolo, A. Olivas, E. Giorgetti, M. Miranda, *J. Mol. Struc.*, (2009), **936**, 177-186.

(12) Y. Hattori, N. Nishimura, Y. Tsutsui, S. Ghosh,T. Sakurai, K. Sugiyasu, M. Takeuchi, S. Seki, *Chem. Commun.*, (2019), **55**, 13342-13345.

(13) P. Samorí, V. Francke, K. Müllen, J. P. Rabe, *Chem. Eur. J.*, (1999), **5**, 2312-2317.

(14) C. Zhou, T. Liu, T. Lin, X. Zhan, Z. ChenZ, *Polymer*, (2005), **46**, 10952-10959.

(15) UHF. Bunz, V. Enkelmann, L. Kloppenburg, D. Jones, KD. Shimizu, JB. Claridge, *Chem Mater*, (1999), **11**, 1416-1424.

(16) C. Weder, MS. Wrighton, *Macromolecules*, (1996), **29**, 5157-5165.

(17) R. Azumi, G. Giitz, P. Bauerle, *Synthetic Metals*, (1999), **101**, 544-545.

(18) A. Moser, J. Novak, H. Flesch,1 T. Djuric, O. Werzer, A. Haase, R. Resel, *Appl. Phys. Lett.*, (2011), **99**, 221911.

(19) M. D. Curtis, J. I. Nanos, H. Moon, W. Sang Jahng, *J. Am. Chem. Soc.*, (2007), **129**, 15072-15084.

(20) M. Kasha, H. Rawls, M. Ashraf El-Bayoumi, *Pure Appl. Chem.*, (1965), **11**, 371-392.

(21) J. Terao, A. Wadahama, A. Matono, T. Tada, S. Watanabe, S. Seki, T. Fujihara, Y. Tsuji, *Nature Commun.*, (2013), **4**, 1691.

(22) J. Terao, K. Kimura, S. Seki, T. Fujihara, Y. Tsuji, *Chem. Commun.*, (2012), **48**, 1577-1579.

(23) Y. Noguchi, A. Saeki, T. Fujiwara, S. Yamanaka, M. Kumano, T. Sakurai, N. Matsuyama, M. Nakano, N. Hirao, Y. Ohishi, S. Seki, *J. Phys. Chem. B*, (2015), **24**, 7219- 7230.

General Conclusion

In this thesis, the author has studied the correlation between the configuration/conformation and the optoelectronic properties of conjugate polymer and oligomer. The new findings in this thesis are summarized as follows.

In chapter 1, the author achieve a more ordered backbone configuration of PPE with simple substituents instead of chiral substituents that restrict the free rotation of the backbones. The configuration of PPE backbones in solution was studied by electronic absorption spectroscopy and fluorescence spectroscopy of **LPPE** and **CPPE** as soluble PPE derivatives, as a function of temperature. **LPPE** showed a remarkable electronic transition at 2.5 eV below 253 K, exhibiting an ultra-sharp 0-0 transitionband with a FWHM of 74 meV and an ultralow Stokes shift of 161 cm^{-1}. The dramatic change in optical properties suggests an apparent ‘‘electronic conjugation’’ in which there is a steep increase in the persistence length along the backbones, although the extension of the geometrical *q* value is limited to 20%. Considering the quantitative estimation of free energy in terms of oscillator strength and the absence of a sharp 0-0 band when the aggregates were prepared by the addition of a poor solvent, it appears that the small energetic disorder of the conjugated backbone is only realized below 253 K. This phenomenon can be explained by the suppression of rotational motions of the phenylene units in the PPE backbones via the temperature decrease, which accelerates the chain aggregation. The rod-like transition

occurs first, and subsequently the chains assemble into ordered aggregates with the suppression of twisting and rotational motions of the intrachain units.

In chapter 2, alkyl symmetrically (**C6-C6**) and alkyl-fluoroalkyl asymmetrically (**C6-C2F4**, **C6-C1F5**) -substituted polyacetylenes were synthesized. The correlation between the backbone configuration and the difference of aggregation enthalpy in the side chains was investigated by electronic absorption spectra at variable temperature. The total transition dipoles were calculated numerically in the visible range, and the Huang-Rhys factor was used to estimate the conformational disorder of conjugated polymers. As a result, unlikely to the case of **C6-C6**, ordered aggregates of **C6-C2F4** and **C6-C1F5** were confirmed after aging. It was evident that the configuration of the isolated main chains significantly affected the aggregation dynamics. In the case of **C6-C1F5**, a clear kink of the curve plotted with the total transition dipoles against temperature was seen at 220 K and 260 K respectively for before and after aging. The observed shift in the temperature at the kink point supports the formation of the ordered aggregates, where the rod-like chains after aging facilitate the effective aggregation of the polymers at higher temperatures than that of coil forms before aging. The simple introduction of semifluoroalkyl chains was found to serve as an efficient tool for controlling the aggregation behavior of soluble PA derivatives.

In chapter 3, the author focused on conjugate oligomer, which identical conjugated chromophores with shorter chains and no distribution are expected to enrich the crystallinity, and thus simulate the inherent optoelectrical properties of the conjugated backbones. Conjugated oligomers with distinct chain length: trimer (**P3**) and pentamer (**P5**) of phenylene-ethynylene units have been

investigated in this work to lead ordered crystalline phases of the linear chain molecules, and serendipitously unique phase transition only in the pentamer was found. Unlike the case of crystalline-liquid crystalline phase transition, the pentamer revealed to show unique solid-solid transition with uniaxial expansion in its condensed phase. TRMC measurement suggests an interplay of the thermal activation of charge carriers enhancing their hopping probability and the uniaxial expansion reducing electronic coupling in π-stacking of adjacent molecules.

Through these studies, the author has developed optoelectric properties of structurally confined conjugate molecules and molecular aggregate. Ordered aggregate structure is promoted by the rod-like chains, temperature modulation and semifluoroalkyl side chains are efficient tool for elongation on the persistence length. The finding demonstrated in this thesis would give a general strategy to stabilize a particular conformer of polymer for practical applications.

List of Publications

Chapter 1

Rod-like transition first or chain aggregation first? ordered aggregation of rod-like poly(p-phenyleneethynylene) chains in solution

Y. Hattori, N. Nishimura, Y. Tsutsui, S. Ghosh,T. Sakurai, K. Sugiyasu, M. Takeuchi, S. Seki, *Chem. Commun.*, (2019), **55**, 13342-13345.

https://pubs.rsc.org/en/content/articlelanding/2019/cc/c9cc06892a

Chapter 2

Impact of Unsymmetrical Alkyl−Fluoroalkyl Side Chains over Coilto- Rod Transition of Soluble Polyacetylenes: Modulation of Electronic Conjugation of Isolated Chains and Their Self Assembly

Y. Motomura, Y. Hattori, T. Sakurai, S. Ghosh and S. Seki, *Macromolecules*, (2019), **52**, 4916–4925.

https://pubs.acs.org/doi/full/10.1021/acs.macromol.9b00629

Chapter 3

Solid-solid transition of microcrystalline oligo(phenylene ethynylene)s: Impact of crystalline structure on optoelectronic properties

Y. Hattori, W. Matsuda, S. Seki, *Chemical Physics Letters*, (2022), **801**,139709.

https://www.sciencedirect.com/science/article/pii/S0009261422003761

Acknowledgments

The author would like to express his deepest gratitude to Professor Shu Seki for his valuable suggestions, helpful discussion and continuous encouragement through the course of his studies.

The author wishes to express his sincere gratitude to Dr. Wakana Matsuda for her kind help in several measurements. He would like to thanks Dr.Tsuneaki Sakurai and Dr. Yusuke Tsutsui for teaching how to synthesis and measure in laboratory. He wishes to thank Professor Kazunori Sugiyasu for his valuable comments and discussion.

He wishes to thank Mr. Yoshihiro Motomura for his collaborations, his respectful experiment helped the author. Acknowledgment is also made to for Ms. Nozomi Nishimura, Mr. Yuichiro Ono, and Mr. Naoto Yakahashi for their collaborations.

The author heartily thanks Ms. Yuki Inoue, Mr. Tomohiro Takeuchi, Mr. Jun Inoue, and Ms. Haruka Okamoto for their encouragement. He also thanks other members of Seki laboratory, and the secretary, Ms. Hiromi Kubo and Ms. Shinobu Shinkai.

The author is grateful would like to the Research Fellowships Japan Society for the Promotion of Science for Young Scientists for financial support.

Finally, the author would like to express his sincere gratitude to his parents Kazutaka Hattori and Takako Hattori, his brothers Shunsuke Hattori and Ryosuke Hattori, and his grandparents Yoko Hattori, Osamu Hattori, Fumoto Ito and the late Osamu Ito, and Shiomi Kato, Naoyuki Kato and Shuji Ito for their continuous support, understanding and encouragement.